الجمهورية الجزائرية الديمقراطية الشعبية
PEOPLE'S DEMOCRATIC REPUBLIC OF ALGERIA
وزارة التعليم العالي والبحث العلمي
MINISTRY OF HIGHER EDUCATION AND SCIENTIFIC RESEARCH
جامعة سعد دحلب البليدة1
UNIVERSITY OF SAAD DAHLEB BLIDA 1

كلية العلوم
Faculty of Sciences
دائرة الفيزياء
Department of Physics

MASTER DIPLOMA THESIS
In Physics
Option: Nanophysics

THEME

STUDY OF ELECTRONIC AND OPTICAL PROPERTIES OF SILICON NITRIDE IN CRYSTALLOGRAPHIC PHASES α AND β

Presented by:

Mr Tahar BOUDELLA

Mrs Fedoi BELKAIS

Defensed on 06/10/2019 in front of the jury composed of:

Dr. S.Lafane	MRB	CDTA	President
Dr. N.Ouarab	MRB	CRTSE	Supervisor
Dr. A. Hassein-Bey	MCB	USD. Blida1	Co-Supervisor
Dr. W.Bekhti	MCB	USD. Blida1	Examiner

Blida 1-2018/2019-

Acknowledgments

Praise is to Allah for allowing us to complete this research work, carried out within Semiconductor Technology Research Center for Energetics (CRTSE).

First of all, we thank Almighty Allah for giving us the strength, will, and privilege to study and follow the path of science.

We would like to express our sincere thanks to the thesis director, ***Dr. Nouredine OUARAB****, Senior Researcher at CRTSE, for the help, support, advice, and guidance he has provided to us during these months, which we reiterate our deep gratitude.*

We would also like to thank our co-supervisor of thesis ***Dr. Abdelkader HASSEIN-BEY****, Senior Lecturer at the Saad Dahlab University of Blida-1, for the help of accomplishment of our work, for the scientific and technical training he provided to us, his advice and encouragement.*

We hold to warmly thank ***Dr. Slimane LAFANE****, Senior Researcher at The Center for Development of Advanced Technologies (CDTA), to have accepted to chair the jury of this thesis.*

We hold to present our thanks to ***Dr. Wided BEKHTI****, Senior Lecturer at the Saad Dahlab University of Blida-1, for her willingness to evaluate this thesis.*

We hold highly to express our deep recognition and our gratitude to all professors of the physics department at the Saad Dahlab University, for all they have given us.

We would like to thank all those who helped us in any way during our stay at the CRTSE research center.

We gratefully acknowledge to our families who always encouraged us to pursue our scientific way to this distant point and supporting us spiritually throughout this thesis as well as throughout our life so far in all its manifestations.

Last but not least, we would like to thanks to all our colleagues at the Saad Dahlab University of Blida-1, all our friends and all the people who encouraged us during these years.

Dedications

I dedicate this work to:

The soul of my mother

My father

My brothers, sisters, and their children

The whole family

My partner in this research work

My friends

TAHAR

Dedications

I dedicate this work to:

My very dear parents

for their sacrifices and their efforts

My husband Hamza

for his support and his encourage

My brothers and sisters

My partner in this work

All my friends

To everyone I love

FEDOI

Abstract

We have performed a systematic study based on density functional theory (DFT) using linearized augmented plane wave method (FP-LAPW) for the calculation of the electronic and optical properties of silicon nitride (Si_3N_4) in both α and β crystallographic phases. But before we do that, structural optimization has been treated calling the Birch-Murnaghan equation of state and the Hellmann-Feynman forces minimization has been done calling the Perdew-Burke-Ernzerhof potential within the generalized gradient approximation (PBE-GGA). The results have shown that electronic behavior can be affected by the variation in lattice parameters, which is viewing in bands structure and density of states spectra, knowing that all electronic properties have been evaluated using the modified Tran-Blaha potential with the local density approximation (LDA). The optimization of electronic properties has indicated that in pure silicon nitride the orbital hybridization can give the appropriate optical properties for photovoltaic application.

So, in pure silicon nitride, the strong orbital hybridization leads to the large bandgap and weedy optical properties in the visible range. But after doping with Al or P as required, the calculation exhibits hoping results leading to the increase of the absorption coefficient and, in general, the optical properties.

Keywords: silicon nitride, ab-initio calculation, band gap, and dielectric tensor

ملخص

لقد أجرينا دراسة منهجية تستند إلى نظرية الكثافة الوظيفية (DFT) باستخدام طريقة الموجة المستوية المتزايدة خطيا (FP-LAPW) لحساب الخصائص الإلكترونية والبصرية لنيتريد السيليكون (Si_3N_4) في كل من الشبكتين البلوريتين α وβ. ولكن قبل القيام بذلك، تمت معالجة التحسين الهيكلي باستدعاء معادلة الحالة لبيرش-مورناغان وتم إجراء تقليل قوات هيلمان-فاينمان إلى أدنى حد ممكن باستدعاء كمون بيردو-بيرك-ايرنزروهف المدمج مع تقريب التدرج المعمم (PBE-GGA). أظهرت النتائج أن التحرك الإلكتروني يمكن أن يتأثر بالتغير في معلمات الشبكة، والذي يتم عرضه في بنية شريط الطاقة وأطياف كثافة الحالات، مع العلم أنه تم تقييم جميع الخصائص الإلكترونية باستخدام كمون تران-بلاها المعدل مع تقريب الكثافة المحلية (LDA). وقد أشار تحسين الخصائص الإلكترونية إلى أنه في نيتريد السيليكون النقي، يمكن للتهجين المداري أن يعطي خصائص بصرية مفيدة للتطبيق الكهروضوئي.

لذلك، في نيتريد السيليكون النقي، يؤدي التهجين المداري القوي إلى فُرجة نطاقي الطاقة وخصائص بصرية سيئة في المدى المرئي. ولكن بعد الإشابة باستخدام الألومنيوم (Al) أو الفوسفور (P) حسب الحاجة، تظهر الحسابات أملاً في الحصول على نتائج تؤدي إلى زيادة معامل الامتصاص والخصائص البصرية بشكل عام.

كلمات مفتاحية: نيتريد السيليكون، حساب ab-initio، فجوة النطاق، وموتر العزل

Contents

Nomenclature

Frequently used abbreviations:

APW	Augmented Plane Wave
CB	Conduction Band
DFT	Density Functional Theory
DOS	Density of States
E_F	Fermi level
FP-LAPW	Full Potential Linearized Augmented Plane Wave
GGA	Generalized Gradient Approximations
KKR	Kramers–Kronig relations
KS	Kohn-Sham equation
LAPW	Linearized Augmented Plane Wave
LDA	Local Density Approximation
PBE	Perdew Burke Ernzerhof
R_{mt}	Muffin-tin radius
SCF	self-consistent field
TB-mBJ	Tran Blaha modified Becke-Johnson
VB	Valence Band
WC	Wu–Cohen
XC	Exchange-correlation functional

List of figures

List of tables

Introduction

The energy supply and environmental protection has increased the need of alternative energy sources, which is why the research and development of photovoltaic solar cells have increased around the world. The performance of photovoltaic solar cells is closely linked to materials properties from which have been manufactured and many material science problems have arisen concerning the development of efficiency coefficient and less expensive solar cells.

Any semiconductor material in a suitable electronic environment can exhibit properties that could be called "photovoltaic", i.e. the generation of electrical current and a difference in potential under illumination. However so few materials are known to form photovoltaic devices with sufficient efficiency to make them potentially interesting for practical applications [1]. Semiconductors are a group of materials with conductivities between those of metals and insulators. Two general classifications of semiconductors are elementary semiconductor materials, which are found in Group IV of the periodic table (Si, Ge, Sn...), and compound materials, most of which are made up of special combinations of elements from Group III (Ga, In, B) and Group V (As, Sb, P) [2]. Among the semiconductor combinations, we have the silicon nitride (Si_3N_4), which can be found in two stable crystal structures; α and β. The local bond is similar in both cases, differing by the number of atoms in the primitive cell.

Silicon nitride is a material of great technological interest due to its mechanical and electronic properties that make it suitable for several applications. Silicon nitride has a high density, high melting temperature, low mechanical stress, and strong resistance against thermal shock. It has high dielectric constant, large electronic gap, high-energy barrier for impurity diffusion, and high resistance against radiation. These properties led to applications in microelectronic devices as a gate dielectric in thin-film transistors, as a charge storage medium in nonvolatile memories, and in solar cells [3]. As for our interest, we will study the electronic and optical properties of silicon nitride in both crystallographic phases α and β, using them as anti-reflective layers on mono- or multi-crystalline silicon-based solar cells.

The present memory is divided into three chapters. In chapter 1, we will outline the bases on which DFT is based, by discussing the different approximations, while chapter 2 is dedicated to the description of the electronic and optical properties of a semiconductor

through the presentation of the different theoretical framework necessary for the results understanding and interpreting. In chapter 3, we will present the results of our calculation and we will discuss electronic properties such as the band structures and the density of state and optical properties such as the absorption coefficient and refractive indices. The thesis ends up by drawing the main conclusion and providing a perspective concerning the two main subjects discussed.

Chapter I

Density Functional Theory and LAPW Methods

I.1. Introduction

The fundamental basis of understanding the different properties of materials and phenomena relies upon understanding their electronic structure. Indeed, developing theoretical approaches that can accurately describe a system of interacting particles, electrons and nuclei, emerged as a serious challenge encountering theoretical physics. An exact theory for a system of ions and interacting electrons is intimately based on quantum mechanical theory for solving a many-body Schrödinger equation itself is complex. The density-functional theory is one of the most popular and successful quantum mechanical approaches to the matter. It is nowadays routinely applied for calculating, e.g., the binding energy of molecules in chemistry, the band structure of solids, superconductivity, atoms in the focus of strong laser pulses, relativistic effects in heavy elements and atomic nuclei, classical liquids, and magnetic properties of alloys have all been studied with DFT.

In this chapter, we will outline the bases on which DFT is founded, by discussing the different approximations needed to solve the Schrödinger equation. Next, two types of approximations are used for the evaluation of the exchange-correlation potential and for the definition of the wave functions, being solutions of the Schrödinger equation will be presented. Finally, we introduce the linearized augmented plane wave method, which is the most accurate method for calculating the electronic structure of solids in density functional theory.

I.2. Density functional theory (DFT)

Density functional theory provides a powerful tool for computations of the quantum state of atoms, molecules and solids [1]. Calculations of material properties using density functional theory (DFT) have become a very active field of research in recent years. The basic idea of DFT is to use the electron charge density n(r) as the basic variable instead of the many-electron wave function used in Hartree-Fock theory [2]. The electron density is quite attractive to work with because it contains only three variables, no matter how many electrons are being considered [3].

I.2.1. A problem with N-body

The basic problem in condensed matter theory, which DFT attempts to solve, is how to deal mathematically with the interactions of a large number of particles. If the system we are interested in is an atom or a small molecule, the number of particles is still rather small, but if we are dealing with larger systems, describing the wave function of the system explicitly

becomes infeasible. The solid is a strongly coupled system consisting of two species, electrons and nuclei with Coulomb interaction both between themselves and each other. The Hamiltonian will, therefore, consist of the following terms:

$$\hat{H} = -\frac{\hbar^2}{2}\sum_I \frac{\nabla_I^2}{M_I} + \frac{1}{2}\sum_{I\neq J} \frac{Z_I Z_J e^2}{4\pi\epsilon_0 |\vec{R}_I - \vec{R}_J|} - \frac{\hbar^2}{2m}\sum_i \nabla_i^2 + \frac{1}{2}\sum_{i\neq j} \frac{e^2}{4\pi\epsilon_0 |\vec{r}_i - \vec{r}_j|} - \sum_{i,I} \frac{Z_I e^2}{4\pi\epsilon_0 |\vec{r}_i - \vec{R}_I|} \quad \text{(I. 1)}$$

Where the indices *i*, *j* are used for electrons and *I*, *J* are for atomic nuclei, M_I denotes nuclear masses, m is the electron mass, $\vec{R}_I$ and $\vec{r}_i$ stand for nuclear and electron coordinates, respectively, and Z_I denotes atomic number [2]. In these systems, one has to deal with the coupled dynamics of electrons and nuclei, i.e. with the Schrödinger equation:

$$\hat{H}\psi_a(R_1, \dots, R_K; r_1, \dots, r_N) = E_a\psi_a(R_1, \dots, R_K; r_1, \dots, r_N) \quad \text{(I. 2)}$$

The size of the systems of interest ranges from atoms to solids so that the particle number in (I.2) varies over many orders of magnitudes. At the same time, a quantum mechanical treatment of the electrons is usually unavoidable, even if only the most elementary features of these systems are to be studied. The standard first step towards a solution of (I.2) is a partial decoupling of the electron from the nuclear motion, which relies on the different time scales of the two types of motion. This is achieved by the Born-Oppenheimer approximation [4].

I.2.2. Born-Oppenheimer approximation

The Schrödinger equation can be further simplified if we take advantage of the significant differences between the masses of nuclei and electrons. Even the lightest of all nuclei, the proton (^{1}H), weighs roughly 1800 times more than an electron. Thus, the nuclei move much slower than the electrons. The practical consequence is that we can take the extreme point of view and consider the electrons as moving in the field of fixed nuclei. This is the famous Born-Oppenheimer or clamped-nuclei approximation [5]. The Born-Oppenheimer approximation amounts to a factorization of the total wave function ψ_a into a nuclear wave function ψ_{ik}^n and an electron wave function ψ_k^e,

$$\psi_{a\equiv i,k}(R_1, \dots, R_K; r_1, \dots, r_N) = \psi_{ik}^n(R_1, \dots, R_K)\psi_k^e(R_1, \dots, R_K; r_1, \dots, r_N) \quad \text{(I. 3)}$$

The electron wave function depends parametrically on the position of the nuclei. It satisfies the Schrödinger equation, [4]

$$\hat{H}_e\psi_k^e(R_1, \dots, R_K; r_1, \dots, r_N) = E_k(R_1, \dots, R_K)\psi_k^e(R_1, \dots, R_K; r_1, \dots, r_N) \quad \text{(I. 4)}$$

Where $\hat{H}_e$ the Hamiltonian acting on the electrons can be written as:

$$\hat{H}_e = -\frac{1}{2}\sum_i \nabla_i^2 + \frac{1}{2}\sum_{i\neq j}\frac{e^2}{|\vec{r}_i - \vec{r}_j|} - \sum_{i,I}\frac{Z_I e^2}{|\vec{r}_i - \vec{R}_I|} = T + W + V_{ext} \qquad (I.5)$$

The first term,T is the kinetic energy operator of the electrons. The second W is the Coulomb potential from electron–electron interaction, and the third term,V_{ext} is the external potential, i.e., the Coulomb potential from the interactions between the electrons and the nuclei. The corresponding total energy E is the expectation value of $\hat{H}_e$ in (I.5), i.e., [2]

$$E = \langle\psi|\hat{H}|\psi\rangle = T + W + \int d^3r V_{ext}(r)n(r) \qquad (I.6)$$

The solution of (I.4) is an arduous computational task, even for fixed positions of the nuclei. Not only the large number and the quantum nature of the electrons represent a challenge, but also the complicated geometry of many systems. It is also possible that several meta-stable arrangements of the nuclei (isomers, conformers) exist so that the solution of (I.4) for each of these arrangements is required to determine the ground state configuration. For these reasons, extremely efficient handling of the electron problem is necessary, even if the possible motion of the nuclei is ignored. A variety of approaches have been developed to obtain approximate solutions of Eq. (I.4). The oldest and simplest is the Hartree-Fock (HF) (or Self-Consistent-Field) approximation, in which the ground state wave function $\psi^e_{k=0}$ is assumed to be a determinant of single-particle states, a so-called Slater determinant [4]. While that the entire field of DFT rests on two fundamental mathematical theorems proved by Kohn and Hohenberg and the derivation of a set of equations by Kohn and Sham in the mid-1960s. The first theorem, proved by Hohenberg and Kohn, is: The ground-state energy from Schrödinger's equation is a unique functional of the electron density [6].

I.2.3. Hohenberg-Kohn theorems

The theorems initially formulated by Hohenberg and Kohn constitute the theoretical basis of DFT. It can be summarized in three statements.

Statement 1 (Uniqueness): The ground-state expectation value of any observable is a unique functional of the exact ground state density $n(r)$.Thus, for example, the ground-state total energy E of a system can always and unambiguously be written as $E[n]$. *Statement 2 (Variational Principle):* The exact ground-state density minimizes the total energy functional $E[n]$. This statement provides us, at least in principle, with a scheme how to

find the ground-state charge density. Simply try all possible densities and choose the one that gives the lowest energy.

Statement 3 (Universality): For the third statement, we need to rewrite our total energy expression (I.6) slightly. The part of the energy functional associated with the external potential can be singled out the remaining terms are summarized in a new functional $F[n]$ containing the kinetic energy and the electron-electron interaction energy. The total energy functional can then be written as:

$$E[n] = F[n] + \int d^3r V_{ext}(r) n(r) \qquad (I.7)$$

The functional $F[n]$ is universal in the sense that it does not depend on $V_{ext}(r)$. Thus, the mathematical form of $F[n]$ will be the same irrespective of system. To proceed further, we follow the path of Kohn and Sham and rewrite the universal functional $F[n] = \mathrm{T[n]} + \mathrm{W[n]}$ as

$$F[n] = T_S[\mathrm{n}] + \frac{1}{2}\int d^3r d^3r' \frac{n(r)n(r')}{|\vec{r} - \vec{r}'|} + E_{xc}[n] \qquad (I.8)$$

The first term, $T_S[\mathrm{n}]$, is the kinetic energy of a hypothetical non-interacting electron gas with the same density, and the second term is easily recognized as the classical Coulomb interaction. The functional $E_{xc}[n]$ is called the exchange and correlation energy. All many-particle effects are contained in $E_{xc}[n]$ [2].

I.2.4. Kohn-Sham equations

The equations of Kohn and Sham, published in 1965, turn DFT into a practical tool. They are a practical procedure to obtain the ground state density [7]. The basic idea of the Kohn–Sham scheme is to map the many-particle problem onto a system of non-interacting particles with the same ground state density $n(r)$ as the original many-particle system. To this end, they perform the variation of the energy functional (I.7) of the many-particle system, with $F[n]$ defined by (I.8):

$$\delta E[n] = 0 \qquad (I.9)$$

and it gives

$$\mu = \frac{\delta E[n]}{\delta n(r)} = V_{ext} + \int d^3r' \frac{n(r')}{|\vec{r} - \vec{r}'|} + \frac{\delta T_S[\mathrm{n}]}{\delta n(r)} + \frac{\delta E_{xc}[\mathrm{n}]}{\delta n(r)} \qquad (I.10)$$

Where μ is the Lagrange multiplier corresponding to the requirement of integer particle number. And they perform the same exercise on the energy functional of a system of non-interacting particles moving in some external potential, say V_{eff}. This energy functional is:

$$E[n] = T_S[n] + \int d^3r V_{eff}(r) n(r) \qquad \text{(I. 11)}$$

And variation gives, expressed in the standard way of writing functional derivatives,

$$\mu = \frac{\delta E[n]}{\delta n(r)} = \frac{\delta T_S[\mathrm{n}]}{\delta n(r)} + V_{eff} \qquad \text{(I. 12)}$$

Where

$$V_{eff} = V_{ext} + \int d^3r' \frac{n(r')}{|\vec{r} - \vec{r}'|} + \frac{\delta E_{xc}[\mathrm{n}]}{\delta n(r)} \qquad \text{(I. 13)}$$

V_{eff} can be looked upon as an effective external potential in which the non-interacting electrons are moving. The last term in (I.13) is called the exchange-correlation potential, i.e.,

$$V_{xc} = \frac{\delta E_{xc}[\mathrm{n}]}{\delta n(r)} \qquad \text{(I. 14)}$$

The effective potential V_{eff} transforms the many-particle problem to a single particle formulation, and the Hamiltonian H_{eff} corresponding to (I.11) is:

$$H_{eff} = -\frac{1}{2}\nabla^2 + V_{eff}(r) \qquad \text{(I. 15)}$$

Which gives a set of coupled Schrödinger-like equations, also called the Kohn–Sham (KS) equations

$$H_{eff}(r)\psi_i(r) = \left[-\frac{1}{2}\nabla^2 + V_{eff}(r)\right]\psi_i(r) = \epsilon_i\psi_i(r), \qquad i = 1, \dots, N \qquad \text{(I. 16)}$$

The ground state density is given by:

$$n(r) = \sum_{i=1}^{N} |\psi_i(r)|^2 \qquad \text{(I. 17)}$$

Where the sum is over the N lowest eigenstates of H_{eff}, and since H_{eff} directly depends on $n(r)$, (I.17) constitutes the coupling between the N one-electron equations in (I.16). With

knowledge of the solution to (I.16), the kinetic energy T_S can be exactly calculated, is given by:

$$T_S = \sum_{i=1}^{N} \left\langle \psi_i \middle| -\frac{1}{2}\nabla^2 \middle| \psi_i \right\rangle = \sum_{i=1}^{N} \epsilon_i - \int d^3r V_{eff}(r) n(r) \qquad \text{(I. 18)}$$

Finally, by combining (I.11), (I.13), (I.14), and (I.18), we obtain the following expression for the total energy [2]:

$$E = \sum_{i=1}^{N} \epsilon_i - \frac{1}{2}\int d^3r d^3r' \frac{n(r)n(r')}{|\vec{r} - \vec{r}'|} - \int d^3r\, V_{xc}[n]n(r) + E_{xc}[n] \qquad \text{(I. 19)}$$

To find the ground-state density, we don't need to use the second Hohenberg-Kohn theorem any more, but we can rely on solving (self-consistent solution) familiar Schrödinger-like non-interacting single-particle equations so called Kohn-Sham equations [7]. However, for the practical calculation, the exchange-correlation energy, which is a functional of the density, requires the introduction of certain approximations.

I.2.5. Exchange-correlation functional

The Kohn-Sham formalism introduced above, allows an exact treatment of most of the contributions to the electronic energy of an atomic or molecular system, including the major fraction of the kinetic energy. All remaining unknown parts are collectively folded into the exchange-correlation functional $E_{xc}[n]$. These include the non-classical portion of the electron-electron interaction along with the correction for the self-interaction and the component of the kinetic energy not covered by the non-interacting reference system. Obviously, the whole endeavor of applying the Kohn-Sham scheme as a tool to get a grip on the Schrödinger equation makes sense only if explicit approximations to this functional are available. The quality of the density functional approach hinges solely on the accuracy of the chosen approximation to E_{xc}. Hence, the quest of finding better functionals is at the very heart of density functional theory. In the following, we will review the current state of the art regarding approximate functionals for E_{xc} [5].

I.2.5.1. Local density approximation (LDA)

In this section, we introduce the model system on which virtually all approximate exchange-correlation functionals are based. At the center of this model is the idea of a hypothetical uniform electron gas. Physically, such a situation resembles the model of an

idealized metal consisting of a perfect crystal of valence electrons and positive cores where the cores are smeared out to arrive at a uniform positive background charge [5]. Since the local density approximation (LDA) is derived from the homogeneous electron gas, one expects that it should work well only for systems with slowly varying densities. The LDA consists of the replacement of the exact $E_{XC}[n]$ by the LDA functional [2]

$$E_{xc}^{LDA}[n] = \int d^3r\, n(\vec{r})\varepsilon_{xc}(n) \qquad \text{(I. 20)}$$

Here, $\varepsilon_{xc}(n)$ is the exchange-correlation energy per particle of a uniform electron gas of density $n(\vec{r})$. This energy per particle is weighted with the probability $n(\vec{r})$ that there is in fact an electron at this position in space. Writing E_{XC} in this way defines the local density approximation. The quantity $\varepsilon_{xc}(n)$ can be further split into exchange and correlation contributions,

$$\varepsilon_{xc}(n) = \varepsilon_x(n) + \varepsilon_c(n) \qquad \text{(I. 21)}$$

The exchange part, ε_x, which represents the exchange energy of an electron in a uniform electron gas of a particular density is, apart from the pre-factor, equal to the form found by Slater in his approximation of the Hartree-Fock exchange [5] and was originally derived by Bloch and Dirac in the late 1920's:

$$\varepsilon_x = -\frac{3}{4}\sqrt[3]{\frac{3n(\vec{r})}{\pi}} \qquad \text{(I. 22)}$$

No such explicit expression is known for the correlation part, ε_c. However, highly accurate numerical quantum Monte-Carlo simulations of the homogeneous electron gas are available from the work of Ceperly and Alder, (1980).On the basis of these results various authors have presented analytical expressions of ε_c based on sophisticated interpolation schemes. The most widely used representations of ε_c are the ones developed by Vosko, Wilk, and Nusair, (1980), while the most recent and probably also most accurate one has been given by Perdew and Wang, (1992).

I.2.5.2. Generalized gradient approximations (GGA)

A general approach in which E_{xc} is assumed to depend in some general way on the charge density and its gradients gives rise to a family of approximations called the generalized gradient approximations (GGA). In many cases these functionals are superior to LDA and have therefore become the most commonly used ones in modern DFT calculations. If we let

the magnitude of the first-order gradient of the density enter the expression, the exchange correlation energy can be written as

$$E_{xc}^{GGA}[n] = \int d^3r\, n(\vec{r}) f(n, |\nabla n|) \qquad (I.23)$$

Where $f(n, |\nabla n|)$ is some function, which is to be modeled so that the resulting functional behaves well according to various criteria. There is some freedom to incorporate the density gradient, and therefore several versions of GGA exist [2]. Two of the most widely used functionals in calculations involving solids are the Perdew–Wang functional (PW91) and the Perdew–Burke–Ernzerhof functional (PBE) [6].

I.2.6. Solving the Kohn-Sham equations

The resolution of the Kohn-Sham equations requires the choice of a basis for the wave functions that can be taken as a linear combination of orbitals called Kohn-Sham orbitals written in the following form:

$$\varphi_i(\vec{r}) = \sum C_{ij} \emptyset_j(\vec{r}) \qquad (I.24)$$

Where $\varphi_i(\vec{r})$ are the basic functions and the C_{ij} are development coefficients.

The resolution of Kohn-Sham equations comes down to the determination of the C_{ij}coefficients for occupied orbitals that minimize the total energy. The resolution of the KS equations for the points of symmetry in the first Brillouin zone makes it possible to simplify the calculations. This resolution is done iteratively using a self-consistent iteration cycle.

I.3. Linearized augmented plane wave (LAPW)

The Linearized Augmented Plane Wave (LAPW) method has proven to be one of the most accurate methods for the computation of the electronic structure of solids within density functional theory. In the following, we will see the basic concepts of the LAPW

I.3.1. Augmented plane wave (APW)

The augmented plane wave (APW) method is exposed by Slater in his article [9]. He assumed that in the region far away from the nuclei, the electrons are more or less ‘free’. Free electrons are described by plane waves. Close to the nuclei, the electrons behave quite as they were in a free atom, and they could be described more efficiently by atomic like functions. Space is therefore divided now in two regions: around each atom, a sphere with radius Rα is drawn (call it Sα). Such a sphere is often called a muffin tin sphere, the part of space occupied by the spheres is the muffin tin region. The remaining space outside the spheres is called the interstitial region (call it I).

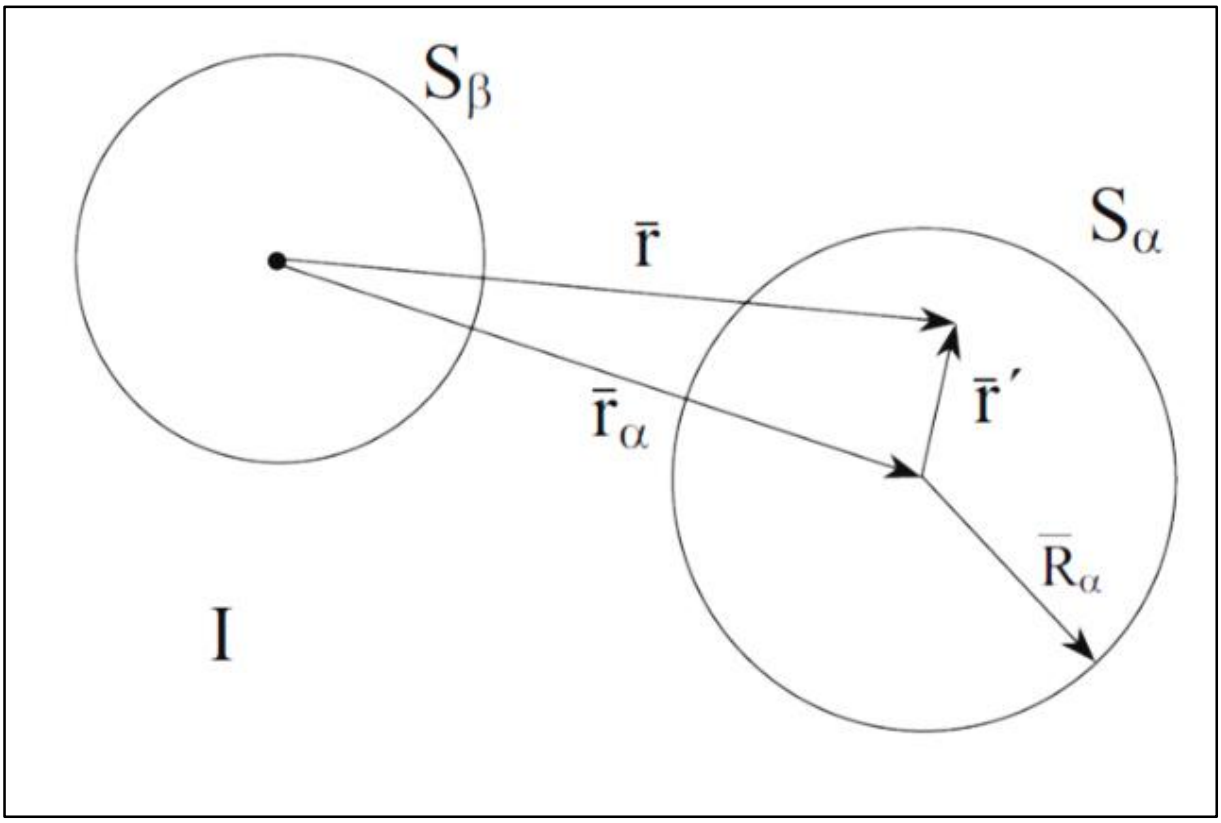

Figure I.1*: Division of a unit cell in muffin tin regions and the interstitial region, for a case with two atoms. The black dot is the origin of the axis system (which may but need not to coincide with the nucleus of an atom)* [7].

One augmented plane wave (APW) used in the expansion of $\psi_{\vec{k}}^{n}$ is defined as:

$$\phi_{\vec{K}}^{\vec{k}}(\vec{r},E)=\begin{cases}\dfrac{1}{\sqrt{V}}e^{i(\vec{k}+\vec{K}).\vec{r}} & \vec{r}\in I\\ \sum_{l,m}A_{lm}^{\alpha,\vec{k}+\vec{K}}u_l^{\alpha}(r',E)Y_m^l(\hat{r}') & \vec{r}\in S_\alpha\end{cases} \qquad \text{(I. 25)}$$

- $\phi_{\vec{K}}^{\vec{k}}(\vec{r},E)$: The wave function
- $A_{lm}^{\alpha,\vec{k}+\vec{K}}$: Coefficient of development in plane waves and spherical harmonic.
- $\vec{k}$: The wave vector in the irreducible Brillouin zone (IBZ).
- $\vec{K}$: Reciprocal lattice vector.
- $\vec{r}'=\vec{r}-\vec{r}_\alpha$: The position inside the spheres.
- V: The volume of the unit cell.
- Y_m^l: Spherical harmonics.
- u_l^α: The u_l^α are solutions to the radial part of the Schrödinger equation for a free atom α, and this at the energy E [7].

The coefficients $A_{lm}^{\alpha,\vec{k}+\vec{K}}$ are chosen such that the atomic functions for all lm components match (in value) the PW with K at the MT sphere boundary. The KS orbitals $\psi_i(r)$ are expressed as a linear combination of APWs $\phi_{\vec{K}}^{\vec{k}}(\vec{r},E)$. Inside the MT sphere a KS orbital can only be accurately described if E in the APW basis functions is equal to the eigen-energy, E_i. Therefore, a different energy-dependent set of APW basis functions must be found for each eigenenergy. This leads to a non-linear eigenvalue problem that is computationally very demanding. One had to choose an energy, solve the radial Schrödinger equation to obtain the APW basis and set up the matrix elements. Then the determinant $|H-ES|$ had to be computed, that should vanish according to the secular equation but did not. So one had to vary the trial energy to numerically find the zeros of this determinant, a procedure complicated by the presence of asymptotes. This was the main drawback of the APW scheme which at best works for simple systems with few eigenvalues only [10].

I.3.2. Linearized augmented plane wave (LAPW)

The problem with the APW method was that the $u_l^{\alpha}(r',E)$ have to be constructed at the – yet unknown – eigenenergy$E=\epsilon_{\vec{k}}^{n}$ of the searched eigenstate. It would be helpful if we were able to recover $u_l^{\alpha}\left(r',\epsilon_{\vec{k}}^{n}\right)$ on the fly from known quantities. That is exactly what the Linearized Augmented Plane Wave method enables us to do. If we have calculated u_l^{α} at some energy E_0, we could make a Taylor expansion to find it at energies not far away from it:

$$u_l^{\alpha}\left(r',\epsilon_{\vec{k}}^{n}\right)= u_l^{\alpha}(r',E_0)+\left(E_0-\epsilon_{\vec{k}}^{n}\right)\dot{u}_l^{\alpha}(r',E_0)+O\left(E_0-\epsilon_{\vec{k}}^{n}\right)^2 \qquad \text{(I. 26)}$$

Substituting the first two terms of the expansion in the APW for a fixed E_0 gives the definition of an LAPW. This has a price: the energy difference $\left(E_0-\epsilon_{\vec{k}}^{n}\right)$ is unknown, and hence a yet undetermined $B_{lm}^{\alpha,\vec{k}+\vec{K}}$ has to be introduced:

$$\phi_{\vec{K}}^{\vec{k}}(\vec{r})=\begin{cases}\dfrac{1}{\sqrt{V}}e^{i(\vec{k}+\vec{K}).\vec{r}} & \vec{r}\in I\\ \displaystyle\sum_{l,m}\left(A_{lm}^{\alpha,\vec{k}+\vec{K}}u_l^{\alpha}(r',E_0)+B_{lm}^{\alpha,\vec{k}+\vec{K}}\dot{u}_l^{\alpha}(r',E_0)\right)Y_m^l(\hat{r}') & \vec{r}\in S_{\alpha}\end{cases} \qquad \text{(I. 27)}$$

In order to determine both $A_{lm}^{\alpha,\vec{k}+\vec{K}}$ and $B_{lm}^{\alpha,\vec{k}+\vec{K}}$, we will require that the function in the sphere matches the plane wave both in value and in slope at the sphere boundary. Equation (I.27) is not the final definition of an LAPW yet. Imagine we want to describe an eigenstate $\psi_{\vec{k}}^{n}$ that has predominantly p-character ($l=1$) for atom α. This means that in its expansion in

LAPW's, the $A_{(l=1)m}^{\alpha,\vec{k}+\vec{K}}$ are large. It is therefore advantageous to choose E_0 near the centre of the p-band. In this way, the $O\left(E_0-\epsilon_{\vec{k}}^{n}\right)^2$ term in equation (I.26) will remain small, and cutting after the linear term is certainly allowed. We can repeat this argument for every physically important l (s-, p-, d- and f-states, i.e. up to l=3) and for every atom. As a result, we should not choose one universal E_0, but a set of well chosen $E_{1,l}^{\alpha}$ up to l=3. The final definition of an LAPW is then:

$$\phi_{\vec{K}}^{\vec{k}}(\vec{r})=\begin{cases}\dfrac{1}{\sqrt{V}}e^{i(\vec{k}+\vec{K}).\vec{r}} & \vec{r}\in I\\ \sum_{l,m}\left(A_{lm}^{\alpha,\vec{k}+\vec{K}}u_l^{\alpha}\left(r',E_{1,l}^{\alpha}\right)+B_{lm}^{\alpha,\vec{k}+\vec{K}}\dot{u}_l^{\alpha}\left(r',E_{1,l}^{\alpha}\right)\right)Y_m^l(\hat{r}') & \vec{r}\in S_\alpha\end{cases} \qquad (I.28)$$

With the $E_{1,l}^{\alpha}$ being fixed, the basis functions can be calculated once and for all. The same procedure as used for the plane wave basis set can now be applied. One diagonalization will yield P different band energies for this $\vec{k}$ [7].

I.3.3. Full potential linearized augmented plane wave (FP-LAPW)

In the Full Potential Linearized Augmented Plane Waves (FP-LAPW) method [11], no approximation is made for the form of the potential or the charge density. These are rather developed into lattice harmonics inside each atomic sphere, and in Fourier series in the interstitial regions; which is at the origin of the name Full-Potential. This method thus ensures the continuity of the potential at the surface of the sphere MT and develops it in the following form:

$$V(\vec{r})=\begin{cases}\sum_K V_K e^{i\vec{K}\vec{r}} & \vec{r}\in I\\ \sum_{lm}V_{lm}(\vec{r})Y_{lm}(\vec{r}) & \vec{r}\in S_\alpha\end{cases} \qquad (I.29)$$

In the same way, the charge density is developed in the form:

$$\rho(\vec{r})=\begin{cases}\sum_K \rho_K e^{-\vec{K}\vec{r}} & \vec{r}\in I\\ \sum_{lm}\rho_{lm}(\vec{r})Y_{lm}(\vec{r}) & \vec{r}\in S_\alpha\end{cases} \qquad (I.30)$$

This method is very accurate, widely used, with a reasonable computing efficiency to simulate the properties of materials based on Density Functional Theory (DFT).

I.4. Wien2k simulation package

All theoretical work done or in progress has a goal, that of predicting new materials or systems that meet current technological needs. Thus, several calculation programs are developed, such as CRYSTAL, Wien2k, VASP, ABINIT, etc. The point of difference between these programs lies in the choice of the basis of development.

The Wien2k code is an implementation of the FP-LAPW method. This program was created by Blaha and his collaborators [8]. It is consists of several independent programs linked by the c-shell scripts. The calculation is done in three steps:

1- Initialization:

To determine the properties of a given material, it is necessary to generate the starting data found in the file "case.struct". This latter contains the lattice parameter, the crystalline structure, the muffin-tin radius, the symmetry operations…etc. This step is done for the preparation of the SCF cycle. These elements are generated by a series of small programs:

- **NN:** This program calculates the nearest neighbor distances of all atoms, and checks that the corresponding atomic spheres (radii) are not overlapping.
- **SGROUP:** This program uses information from "case.struct" (lattice type, lattice constants, and atomic positions) and determines the space-group as well as all point-groups of non-equivalent sites.
- **SYMMETRY:** This program uses information (lattice type, atomic positions) to generates the space group symmetry operations, determines the point group of the individual atomic sites, generates the LM expansion for the lattice harmonics and local rotation matrices
- **LSTART:** generates atomic densities and determines how the orbitals are treated in the band structure calculations (i.e. as core or band states, with or without local orbitals).
- **KGEN:** generates a k-mesh in the Brillouin zone (BZ).
- **DSTART:** generates a starting density for the SCF cycle by superposition of atomic densities generated in lstart.

2- SCF calculation:

- **LAPW0:** computes the total potential V_{tot} as the sum of the Coulomb V_c and the exchange-correlation potential V_{xc} using the total electron density as input.

- **LAPW1**: sets up the Hamiltonian and the overlap matrix and finds by diagonalization eigenvalues and eigenvectors.
- **LAPW2:** computes valence densities from eigenvectors
- **LCORE:** computes core states and densities
- **MIXER:** mixing the output density with the input density (the electron densities of core, semi-core, and valence states) to obtain the new density to be used in the next iteration.

3- Calculating properties:

Once the SCF cycle has converged one can calculate various properties like Density of States (DOS), band structure or Optical properties. The calculation of the physical properties is done by means of the programs:

- **OPTIMIZE:** determines the total energy as a function of the volume used to calculate the lattice parameter, the compressibility module and its derivative.
- **TETRA:** This program calculates total and partial density of states (DOS).
- **SPAGHETTI:** calculates the band structure using the eigenvalues generated by LAPW1.
- **OPTIC:** calculates the optical properties.
- **XSPEC:** This program calculates near edge structure of x-ray absorption or emission spectra [8].

Chapter II

Optical and Electronic Properties of Semiconductors

II.1. Introduction

This chapter is dedicated to the description of the electronic and optical properties of a semiconductor, we will present the different theoretical notions necessary for understanding and interpreting. At first, we will discuss the electronic properties (the band structures, the density of state, the electrical conductivity…), next, the optical properties such as absorption coefficient, refractive indices, etc.

II.2. Electronic properties

II.2.1. Band structure

The band structure of semiconductors emerges as a solution of Schrodinger's equation for no interacting electrons in the periodic potential of the crystal lattice:

$$\left[-\frac{\hbar^2}{2m_e}\Delta + U(\vec{r})\right]\psi(\vec{r}) = E\,\psi(\vec{r}) \qquad \text{(II. 1)}$$

Where the potential has the property

$$U(\vec{r}) = U(\vec{r} + \vec{R}) \qquad \text{(II. 2)}$$

The vector R is an arbitrary translation vector that moves the lattice onto itself [1]. For all vectors R of the direct lattice, the potential is due to the effect of the ion cores and all other electrons. Thus a serious many-body problem is present. In principle, the band structure can be calculated from the periodic arrangements of the atoms and their atomic order number. We note that for some problems, e.g. the design of optimal solar cells, a certain band structure is known to be ideal and a periodic atomic arrangement, i.e. a material, needed to be found that generates the optimal band structure. This problem is called the inverse band structure problem [2].

The problem of band structure becomes greatly simplified if we are dealing with crystalline materials. An electron in a rigid crystal structure sees a periodic background potential. As a result, the wave function for electron satisfies Bloch's theorem discussed in the next section [3].

II.2.2. Bloch theorem

We will deduce some general conclusions about the structure of the solution as a consequence of the periodicity of the potential. We first investigate the solution of a Schrodinger equation of the type

$$H\Psi(\vec{r}) = \left[-\frac{\hbar^2}{2m}\nabla^2 + U(\vec{r})\right]\ \psi(\vec{r}) = \ E\,\psi\,(\vec{r}) \qquad \text{(II. 3)}$$

For an electron, $U(\vec{r})$ will be periodic with the lattice.

Bloch's theorem says that the eigenstates Ψ of a one-particle Hamiltonian as in (II.3) can be written as the product of plane waves and a lattice-periodic function, i.e.

$$\Psi_{nk}\,(\vec{r}) = Ae^{i\vec{k}\vec{r}}u_{nk}(\vec{r}) \qquad \text{(II. 4)}$$

The normalization constant A is often omitted. If is normalized, A = $1/\sqrt{V}$ where V is the integration volume. The wave function is indexed with a quantum number n and the wave vector $\vec{k}$. The key is that the function the so-called Bloch function, is periodic with the lattice, i.e.

$$u_{nk}(\vec{r}) = u_{nk}\left(\vec{r} + \vec{R}\right) \qquad \text{(II. 5)}$$

For all vectors $\vec{R}$ of the direct lattice, the proof is simple in one dimension and more involved in three dimensions with possibly degenerate wave functions. If E_{nK} is an energy eigenvalue, then E_{nK+G} is also an eigenvalue for all vectors *G* of the reciprocal lattice, i.e.

$$E_n\left(\vec{K}\right) = E_n\left(\vec{K} + \vec{G}\right) \qquad \text{(II. 6)}$$

Thus the energy values are periodic in reciprocal space. The proof is simple, since the wave function (for $\vec{K} + \vec{G}$) $exp\left(i\left(\vec{K} + \vec{G}\right)\vec{r}\right)u_{n(\vec{K}+\vec{G})}(r)$ is for $\mathrm{u_{n(\vec{K}+\vec{G})}(r) = \exp\left(-i\vec{G}\vec{r}\right)u_{nk}(\vec{r})}$ obviously an eigenfunction to k [2].

II.2.3. Free-electron dispersion

If the entire wave function (from (II.4)) obeys the Schrödinger equation (II.3), the Bloch function u_{nk} fulfills the equation:

$$\left[-\frac{1}{2m}(P + K)^2 + U(\vec{r})\right]u_{nK}(\vec{r}) = \ E_{nK}u_{nK}(\vec{r}) \qquad \text{(II. 7)}$$

Which is easy to see from $\vec{p} = -i\hbar\vec{\nabla}$ periodic potential, U ≡ 0 (this calculation is also called the empty lattice calculation) the solution of (II.7) is then just constant, i.e. $\vec{u}_k = c$ and $\psi_K(\vec{r}) = c\, exp(i\vec{k}\vec{r})$ dispersion of the free electron is then given by

$$E(\vec{K}) = \frac{\hbar^2}{2m}K^2 \qquad \text{(II. 8)}$$

Where $\overrightarrow{K}$ is an arbitrary vector in the reciprocal space, $\vec{K}'$ is a vector from the Brillouin zone such that $K = K' + G$ with a suitable reciprocal lattice vector *G*. Because of (II.6) the dispersion relation can be written also as

$$E(\vec{K}) = \frac{\hbar^2}{2m}(K' + G)^2 \qquad \text{(II. 9)}$$

Where $\overrightarrow{K'}$ denotes a vector from the Brillouin zone. Thus, many branches of the dispersion relation arise from using various reciprocal lattice vectors in (II.9) [2].

II.2.4. Methods of band structure calculation

There are two main categories of realistic band structure calculation for semiconductors.

- Methods which describe the entire valence and conduction bands (techniques such as the, the pseudopotential method and the orthogonalized plan wave methods).

- Methods which describe near band-edge band structure. (Perturbative technique K.P method is simple and considerably more accurate if one is interested only in phenomena near the band-edges.) [3].

II.2.4.1. The pseudopotential method

The pseudopotential method for calculating the energy structure in crystals is based on the fact that conduction and valence states must be orthogonal to the core states. The effect of orthogonality however is used to further the development of approximation or interpolation procedures. A conduction or valence state satisfies the Schrödinger equation [4]:

$$\left[-\frac{\hbar^2}{2m}\nabla^2 + V(\vec{r})\right]\psi_n(\vec{r}) = E_n(\vec{k})\psi_n(\vec{r}) \qquad \text{(II. 10)}$$

However, it is possible only when we know the crystal potential $V(\vec{r})$. In the following we will show how the Schrödinger equation is solved to a good approximation by using empirical parameters, known as pseudopotentials, and the orthogonality of the wave functions.

First, we assume the electron wave functions of the core states and their energies are given by Φ_j and E_j respectively. We then have

$$H|\Phi_j\rangle = [H_0 + V(\vec{r})]\,|\Phi_j\rangle = E_n|\Phi_j\rangle \qquad \text{(II. 11)}$$

Where: $H_0 = -\frac{\hbar^2}{2m}\nabla^2$

The Bloch functions $|\psi\rangle$ of the electrons in the valence and conduction band are orthogonal with the above wave functions $|\Phi_j\rangle$; in other words, we have the following relation $\langle\Phi_j|\psi\rangle = 0$

The above orthogonality is satisfied when we choose the wave functions given by

$$|\psi(\vec{k}.\vec{r})\rangle = |\chi_n(\vec{k}.\vec{r})\rangle - \sum_j \langle\Phi_j|\chi_n\rangle\,|\Phi_j\rangle \qquad \text{(II. 12)}$$

This is evident from the relation

$$\langle\Phi_{j'}|\psi\rangle = \langle\Phi_{j'}|\chi_n\rangle - \sum_j \langle\Phi_j|\chi_n\rangle\langle\Phi_{j'}|\Phi_j\rangle$$

$$= \langle\Phi_{j'}|\chi_n\rangle - \sum_j \langle\Phi_j|\chi_n\rangle\delta_{j'j} \equiv 0 \qquad \text{(II. 13)}$$

Substituting (II.12) into (II.10) we find

$$H|\chi_n\rangle - \sum_j \langle\Phi_j|\chi_n\rangle H\,|\Phi_j\rangle = E_n(k)\left\{|\chi_n\rangle - \sum_j \langle\Phi_j|\chi_n\rangle\,|\Phi_j\rangle\right\} \qquad \text{(II. 14)}$$

And then we obtain the following relation

$$H|\chi_n\rangle + \sum_j \big[E_n(k) - E_j\big]|\Phi_j\rangle\langle\Phi_j|\chi_n\rangle = E_n(k)|\chi_n\rangle$$

New parameter: $V_p = \sum_j \big[E_n(k) - E_j\big]|\Phi_j\rangle\langle\Phi_j|$

Will lead to $\big[H + V_p\big]|\chi_n\rangle = E_n(k)|\chi_n\rangle$

Or

$$\big[H_0 + V(\vec{r}) + V_p(\vec{r})\big]|\chi_n\rangle = E_n(k)|\chi_n\rangle \qquad \text{(II. 15)}$$

Where, $E_n(k)$ is the band energy, which we are interested in. There exists the following inequality between the energies of the core states, E_j, and the energies of the valance and conduction bands, $E_n(k)$: $E_n(k) > E_j$

And thus we find that: $V_p > 0$

we may rewrite (II.15) as

$$\left[H_0 + V_{ps} \right] |^{\chi}_n\rangle = E_n(k) |^{\chi}_n\rangle \quad \text{(II. 16)}$$

$$V_{ps} = V(\vec{r}) + V_p(\vec{r}) \quad \text{(II. 17)}$$

And it may be possible to make V_{ps} small enough, since $V(\vec{r}) < 0$. The new potential $V_{ps}(\vec{r})$, called the pseudopotential, is also periodic, and we can expand it as the Fourier series [4]:

$$V_{ps}(\vec{r}) = \sum_j V_{ps}(\vec{G}_j) e^{-i \vec{G}_j . \vec{r}} \quad \text{(II. 18)}$$

II.2.4.2. The K.P method

If we substitute a Bloch function into the Schrödinger equation:

$$-\frac{\hbar^2}{2m} \nabla^2 \psi(r) + V(r)\, \psi(r) = E\, \psi(r) \quad \text{(II. 19)}$$

We obtain the equation for the periodic part

$$\left[\frac{P^2}{2m} + \frac{\hbar}{m} \vec{k}.\vec{p} + \frac{\hbar^2 k^2}{2m} + V(\vec{r}) \right] u_{nk}(\vec{r}) = E_n(\vec{k}) u_{nk}(\vec{r}) \quad \text{(II. 20)}$$

Where the band index n has been added at $\vec{k}$ = 0, the above equation becomes the same equation satisfied by the total wave-function:

$$\left(\frac{P^2}{2m} + V(\vec{r}) \right) u_{n0}(\vec{r}) = E_n(\vec{k}) u_{n0}(\vec{r}) \quad \text{(II. 21)}$$

If we are interested in the electronic states near $\vec{k}$ = 0 (point Γ), the two terms containing $\vec{k}$ in (II.20) can be treated as a perturbation. For this, however, we need the eigenfunctions at Γ. On the other hand, (II.21) for such functions is much easier to solve than the general Schrödinger equation. As expected, the states obtained with this method are rather good for small $\vec{k}$, although the method can be extended to expand the band structure around any given value k. In particular, the effective masses (i.e., the curvatures of the bands around their minima), obtained with this method, with simple approximations for the wave functions at Γ, are in good agreement with the experimental values [5].

II.2.5. Density of states

The dispersion relation yields how the energy of a (quasi-) particle depends on the $\vec{k}$ vector. Now we want to know how many states are at a given energy. This quantity is called

the density of states (DOS) and is written as $D(E)$. It is defined in an infinitesimal sense such that the number of states between E and $E + \delta E$ *is* $D(E)\delta E$. In the vicinity of the extrema of the band structure many states are at the same energy such that the density of states is high. The dispersion relation of a band will be given as $E = E(\vec{k})$. If several bands overlap, the densities of state of all bands need to be summed up. The density of states at the energy E' for the given band is

$$(E')dE = 2\int \frac{d^3k}{\left(\frac{2\pi}{L}\right)^3}\delta\left(E' - E\left(\vec{k}\right)\right) \qquad \text{(II. 22)}$$

Where $(2\pi/L)^3$ is the k-space volume for one state. The factor 2 is for spin degeneracy. The integral runs over the entire k-space and selects only those states that are at E'. The volume integral can be converted to a surface integral over the isoenergy surface $S(E')$ with $E\left(\vec{\mathrm{k}}\right) = E'$ the volume element $\mathrm{d}^3\mathrm{k}$ is written as $\mathrm{d}^2\mathrm{S}dk_\perp$. The vector $k_\perp$is perpendicular to $S(E')$ and proportional to $\nabla_K E(\vec{k})$, i.e. $\mathrm{dE} = \left|\nabla_K E(\vec{k})\right| d\vec{k}_\perp$

$$D(E') = 2\int_{S(E')} \frac{d^2S}{\left(\frac{2\pi}{L}\right)^3}\frac{1}{|\nabla_K E(k)|} \qquad \text{(II. 23)}$$

In this equation, the dispersion relation is explicitly contained. At band extrema, the gradient diverges in three dimensions in which singularities are integrable and the densities of states take finite values. The corresponding peak is named a Van Hove singularity. The concept of the density of states is valid for all possible dispersion relations, e.g. for electrons, phonons or photons [2].

II.2.6. Transport electron phenomena

II.2.6.1. Electron and hole in semiconductors

In a semiconductor containing no impurities or defects, i.e., an intrinsic semiconductor, at temperatures above 0 K some thermally excited electrons are promoted from the valence band to the conduction band. An unoccupied state in the valence band is called a hole, which may be regarded as a positive charge carrier that can contribute to the conduction process. Electronic transitions across the energy gap to the conduction band result in a spontaneous generation of holes in the valence band, and the generated carriers are described as electron–hole pairs. After a random motion through the lattice, the electron in the conduction band

encounters a hole and undergoes a recombination transition. The generation of electron–hole pairs and their subsequent recombination is a continuous process, and the average time that carriers exist between generation and recombination is called the lifetime of the carrier. During this process of generation of electron–hole pairs, the concentration of electrons (denoted as n) in the conduction band is equal to the concentration of holes (denoted as p) in the valence band. This can be expressed as $n = p = n_i$ where, n_i is the intrinsic carrier concentration.

Electrons and holes in the conduction and valence bands, respectively (carrying negative and positive electronic charges, respectively), are referred to as free charge carriers. In the presence of an electric field the free charge carriers attain the drift velocity v, and a net current density j [6].

II.2.6.2. Current density

The equation of motion for the electron in the band structure is no longer given by Newton's law $F = d(mv)/dt$ as in vacuum. Instead, the propagation of quantum-mechanical electron wave packets has to be considered. Their group velocity is given by

$$\vartheta_g = \frac{dw}{dk} = \frac{1}{\hbar}\frac{dE}{dk} \qquad \text{(II. 24)}$$

Through the dispersion relation the influence of the crystal and its periodic potential on the motion enters the equation. An electric field ε acts on an electron during the time δt the work $\delta E = -e\varepsilon v g \delta t$. This change in energy is related to a change in k via $\delta E = dE/dk.\,\delta k = \hbar v g \delta k$. Thus, we arrive at $\hbar dk/dt = -e\varepsilon$. For an external force we thus have

$$\hbar\frac{dk}{dt} = -eE \qquad \text{(II. 25)}$$

Under the influence of an electric field the electrons accelerate according to (II.25)

$$F = m^*\frac{dv}{dt} = \frac{\hbar dk}{dt} = qE = -eE \qquad \text{(II. 26)}$$

In the following, *q* denotes a general charge, while *e* is the (positive) elementary charge. After the time *δt* the *k* vector of all conduction electrons (and the center of the Fermi sphere) has been shifted by *δk*

$$\delta k = -e\frac{\delta t}{\hbar} \qquad \text{(II. 27)}$$

In a real semiconductor, at finite temperatures, impurities, phonons and defects (also the surface) will contribute to scattering. In the relaxation-time approximation it is assumed that the probability for a scattering event, similar to friction, is proportional to the (average) carrier velocity. The average relaxation time τ is introduced via an additional term $\dot{v} = -v/\tau$ that sums up all scattering events. Thus, the maximum velocity that can be reached in a static electric field is given by (steady-state velocity)

$$V = -\frac{eE\tau}{m^*} \qquad \text{(II. 28)}$$

The current density per unit area is then linear in the field, i.e. fulfills Ohm's law

$$j = nqv = \frac{ne^2E\tau}{m^*} = \sigma E \qquad \text{(II. 29)}$$

Where *n* is the electron density, *q* the electronic charge, σ the electrical conductivity [2].

II.2.6.3. Electrical conductivity

It is the ratio between the density of current and the intensity of the electric field, according to the equation (II.29), the electrical conductivity define as

$$\sigma = \frac{\mathrm{ne}^2\tau}{\mathrm{m}^*} \qquad \text{(II. 30)}$$

II.2.6.4. Conductivity tensor

The electrical mobility μ is:

$$\mu = \frac{e\tau}{m^*} \qquad \text{(II. 31)}$$

Substituting (II.31) in (II.29) we find

$$j = ne\mu E = \sigma E \qquad \text{(II. 32)}$$

With components (j_x, j_y, j_z) where

$$\begin{cases} j_x = ne\mu_1 E_x \\ j_y = ne\mu_2 E_y \\ j_z = ne\mu_3 E_z \end{cases} \qquad \text{(II. 33)}$$

The electrical conductivity is thus a tensor, in this case a diagonal one through special choice of axes. If we write [7]:

$$j_r = \sum_s \sigma_{rs} E_S \qquad \text{(II. 34)}$$

With $r, s = x, y, z$ we have:

$$\left.\begin{matrix} \sigma_{xx} = ne\mu_1 \\ \sigma_{yy} = ne\mu_2 \\ \sigma_{zz} = ne\mu_3 \end{matrix}\right\} \sigma_{xy} = \sigma_{yz} = \sigma_{zx} = 0 \qquad \text{(II. 35)}$$

II.3. Optical properties

II.3.1. Kramers-Kronig relation

The Kramers–Kronig relations (KKR) are relations between the real and imaginary part of the dielectric function. They are of a general nature and are based on the properties of a complex, analytical response function $f(\omega) = f_1(\omega) + if_2(\omega)$ fulfilling the following conditions:

- The poles of $f(\omega)$ are below the real axis.
- The integral of $f(\omega)/\omega$ along a semicircle with infinite radius in the upper half of the complex plane vanishes.
- The function $f_1(\omega)$is even and the function $f_2(\omega)$ is odd for real values of the argument.

The integral of $f(s)/(s-\omega)ds$ along the real axis and an infinite semicircle in the upper half of the complex plane is zero because then path is a closed line. The integral along a semicircle above the pole at $s = \omega$ yields $-\pi i f(\omega)$, the integral over the infinite semicircle is zero. Therefore, the value of $f(\omega)$ is given by

$$f(\omega) = \frac{1}{\pi i} Pr \int_{-\infty}^{+\infty} \frac{f(s)}{s-\omega} ds \qquad \text{(II. 36)}$$

Equating the real and imaginary parts of (II.36) yields for the real part

$$f_1(\omega) = \frac{1}{\pi} Pr \int_{-\infty}^{+\infty} \frac{f_2(s)}{s-\omega} ds \qquad \text{(II. 37)}$$

Splitting the integral into two parts $\int_0^{\infty}$ and $\int_{-\infty}^{0}$ going from s to $-s$ in the latter and using $f_2(-\omega) = -f_2(\omega)$ and $\frac{1}{s-\omega} + \frac{1}{s+\omega} = \frac{2}{s^2-\omega^2}$ yields (II.38.a)

$$f_1(\omega) = \frac{2}{\pi} Pr \int_0^{+\infty} \frac{s f_2(s)}{s^2-\omega^2} ds \qquad \text{(II. 38. a)}$$

$$f_2(\omega) = -\frac{2}{\pi} Pr \int_0^{+\infty} \frac{f_1(s)}{s^2-\omega^2} ds \qquad \text{(II. 38. b)}$$

In a similar way, (II.38.b) is obtained. These two relations are the Kramers–Kronig relations. They are most often applied to the dielectric function ε. In this case, they apply to the susceptibility, i.e. $f(\omega) = x(\omega) = \varepsilon(\omega)/\varepsilon_0 - 1$. The susceptibility can be interpreted as the Fourier transform of the time-dependent polarization in the semiconductor after an infinitely short pulsed electric field, i.e. the impulse response of the polarization. For the dielectric function $\varepsilon = \varepsilon_1 + i\varepsilon_2$, the following KK relations hold [2]:

$$\varepsilon_1(\omega) = \varepsilon_0 + \frac{2}{\pi} Pr \int_0^{+\infty} \frac{s\varepsilon_2(s)}{s^2 - \omega^2} ds \qquad \text{(II. 39. a)}$$

$$\varepsilon_2(\omega) = -\frac{2\omega}{\pi} Pr \int_0^{+\infty} \frac{\varepsilon_1(s) - \varepsilon_0}{s^2 - \omega^2} ds \qquad \text{(II. 39. b)}$$

II.3.2. Fundamental absorption process

The fundamental absorption process takes place when photons with energies greater than the band gap energy of the semiconductor (i.e., $h\nu \geq E_g$) are absorbed in a semiconductor. This process usually results in the generation of electron–hole pairs in the semiconductor. For most semiconductors, the fundamental absorption process may occur in the UV, visible, and IR wavelength regimes. It is the most important optical absorption process because important photoelectric effects for generating excess electron–hole pairs in a semiconductor are based on such absorption processes. There are two types of optical transition associated with the fundamental absorption process, namely, direct and indirect band-to-band transitions, as shown in Figures II.1 a and b.

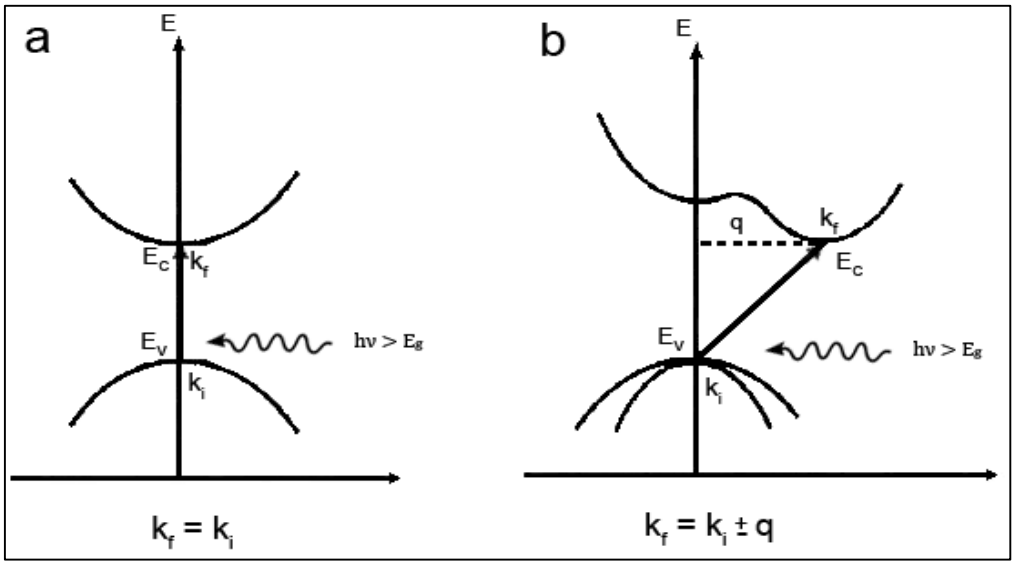

Figure II.1: *Direct and indirect transitions associated with the fundamental absorption processing in a semiconductor* [8].

II.3.2.1. Direct transition process

The direct (or vertical) transition shown in Figure II.1a is the dominant absorption process taking place in a direct band gap semiconductor when the conduction band minimum and the valence band maximum are located at the same k-value in the reciprocal space(i.e., typically at the Γ-point of the Brillouin zone center).

II.3.2.2. Indirect transition process

For an indirect band gap semiconductor, the conduction band minimum and the valence band maximum are not located at the same k-value in the reciprocal space. Therefore, the indirect optical transition induced by photon absorption is usually accompanied by the simultaneous absorption or emission of a phonon. As illustrated in Figure II.1b, conservation of momentum in this case is given by

$$\vec{k}_f = \vec{k}_i \pm \vec{q} \qquad \text{(II. 40)}$$

Where $\vec{k}_f$and $\vec{k}_i$ denote the wave vectors of the final and initial states of electrons, respectively, and $\vec{q}$ is the phonon wave vector. The plus sign in (II.40) corresponds to phonon emission, and the minus sign is for phonon absorption [8].

II.3.3. The absorption coefficient

The optical absorption coefficient is related to the Pointing vector of the electromagnetic (EM) wave energy flow by

$$S(z) = S_0 e^{-\alpha z} \qquad \text{(II. 41)}$$

Where $S(z)$ is the Poynting vector, which is proportional to the square of the amplitude of the electric waves, S_0 is the intensity of the incident beam, z is the length, and α is the optical absorption coefficient.

II.3.3.1. Absorption coefficient for direct transition

The absorption coefficient for a direct allowed transition can be expressed by:

$$\alpha_{da} = K_{da}\left(h\nu - E_g\right)^{1/2} \qquad \text{(II. 42)}$$

Where, K_{da} is a constant.

II.3.3.2. Absorption coefficient for indirect transition

The optical absorption coefficient due to the indirect transitions with phonon absorption is given by:

$$\alpha_{ia}(h\nu) = K_{ia}\frac{\left(h\nu - E_g + \hbar\omega_q\right)^2}{\left(e^{\hbar\omega_q/k_BT} - 1\right)} \quad \text{(II. 43)}$$

Similarly, for transitions involving phonon emission, the optical absorption coefficient can be expressed by:

$$\alpha_{ie}(h\nu) = K_{ie}\frac{\left(h\nu - E_g - \hbar\omega_q\right)^2}{\left(1 - e^{-\hbar\omega_q/k_BT}\right)} \quad \text{(II. 44)}$$

Where $\hbar\omega_q$ is the phonon energy [8].

II.3.4. Refractive index

Many attempts have been made to correlate the energy bandgap to the optical refractive index of semiconductors. Estimation of this parameter is important for optical waveguide in optoelectronic structures like heterojunction laser diodes, optical amplifiers or optical fibers, etc [9].

Moss was the first to find a relation between the refractive index *n* and the energy bandgap E_g based on the atomic model.

$$E_g n^2 = k \quad \text{(II. 45)}$$

Where, k is a constant equal to 108 eV, E_g is the bandgap energy [10].

Ravindra et al proposed a linear relation governing the variation of refractive index with energy gap in semiconductors. The relation is given by [11]:

$$n = 4.084 - 0.62E_g \quad \text{(II. 46)}$$

Herve and Vandamme proposed a model based on the oscillatory theory $\omega \ll \omega_0$

$$n = \sqrt{1 + \left(\frac{A}{E_g + B}\right)^2} \quad \text{(II. 47)}$$

Where: A = 13.6 eV, B = 3.4 eV and ω_0: is the UV resonance frequency [9].

Chapter III

Results and Discussions

III.1. Introduction

In this chapter, we have used the Wien2k code within GGA, LDA, WC, and TB-mBJ-LDA approximations to study the optical and electronic properties of the Si_3N_4 in both crystallographic phases, α and β. In this end, the obtained results from both phases lead to distinguish which phase has better properties to our needs, such as the optical absorption under visible range. Besides, we are going to dope with P or Al the structure that has the best properties for more optimization.

III.2. Presentation of silicon nitride (Si_3N_4)

Silicon nitride is a non-oxide ceramic material with many applications because of its outstanding high temperature and oxidation-resistant properties. It has been extensively applied to micro-electronics, photo-electronics, mechanics, automobile, solar cells and tools for ceramic cutting and processing [1]. As is known, two stable phases of Si_3N_4, α and β, have been synthesized, both of which have a hexagonal crystal structure [2] in which all Si atoms have tetrahedral bonds to N atoms with a strong covalent character [1]. The lattice parameters of each unit cell are presented in the Tab III.1.

Taking the electronic configuration of atoms: Si: $1s^2 2s^2 2p^6 3s^2 3p^2$ N: $1s^2 2s^2 2p^3$

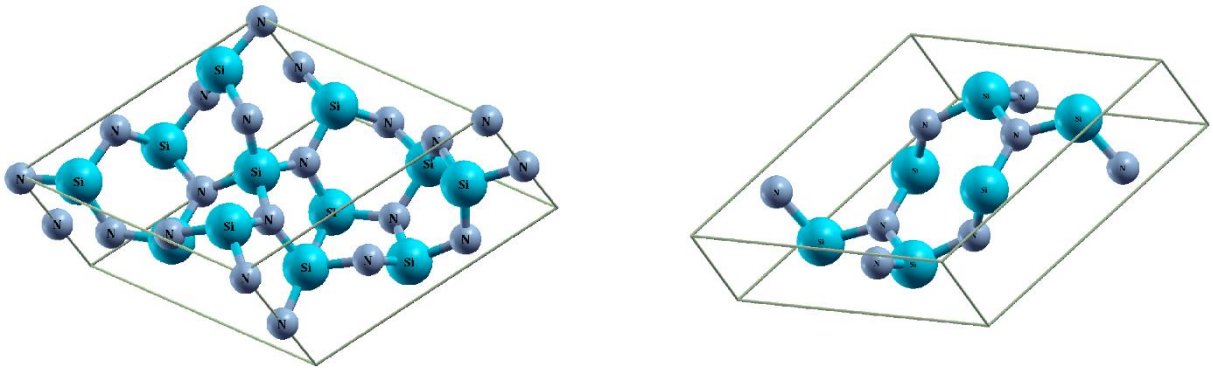

α-Si_3N_4 **β-Si_3N_4**

Figure III.1: *Schematic illustration of Alpha (α-Si_3N_4) and Beta (β-Si_3N_4) structures.*

Parameters / phase	a (Å) x 2	b (Å) x 2	c (Å) x 2	α (°)	β (°)	γ (°)	Space Group
α-Si_3N_4	14.279308	14.279308	10.245155	90	90	120	P31c
β-Si_3N_4	14.374963	14.374963	5.494003	90	90	120	P63/m

Table III.1: *The parameters of the unit cell for alpha and beta phases.*

The both phases alpha and beta of the silicon nitride have a hexagonal crystal structure, Fig III.2 show the first Brillouin zone of the reciprocal lattice for the hexagonal unit cell.

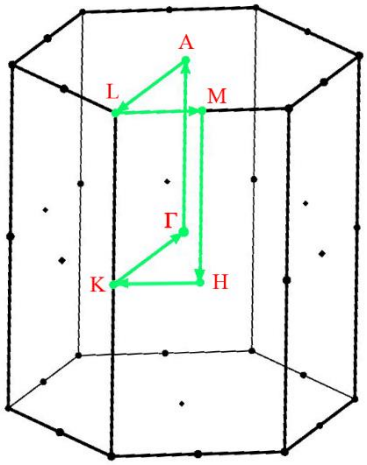

Figure III.2: *The first Brillouin zone of the reciprocal lattice for the hexagonal unit cell.*

III.3. Convergence parameters

We have performed a series of convergence tests within product parameter $R_{mt}\times K_{max}$ to determine a proper cutoff energy value which to be used. Where Rmt is the smallest atomic sphere radius in the unit cell and K_{max} is the maximum module for the reciprocal lattice vector quantified by k special points in FP-LAPW method. In this study, we have chosen muffin-tin radiuses so that there will be no overlap in muffin-tin spheres. The energy, charge and Hellmann-Feynman forces convergence criterions are fixed to 10^{-6} Ry, 10^{-4} C and 0.5 mRy/a.u, respectively. Thus, the R_{mt} was determined as function of energy as it is shown in Fig III.3:

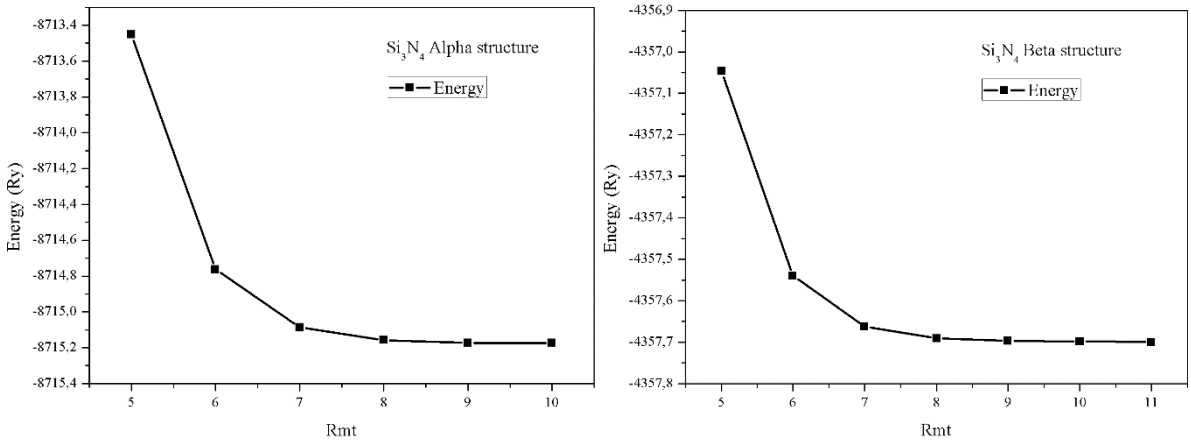

α-Si_3N_4 **β- Si_3N_4**

Figure III.3: *R_{mt} variation as function of total energy for alpha and beta phases.*

Hence, we have fixed the R_{mt} to 9 for both alpha and beta phases with, respectively, 6×6×8 and 4×4×10 of K_{max}.

III.4. Electronic properties

The current step is with great interest to study the electronic behavior of a Si_3N_4 material. But, the use of standard GGA, LDA or WC approximations underestimate the bands structure and, consequently, the density of states. However, a better evaluation of electrical properties can only be achieved through the use of the TB-mBJ-LDA potential, because it yields in most cases results that are in agreement with experiment leading to typical errors of less than 10%.

III.4.1. Band structures

We studied the electronic band structures for the two crystallographic phases, α-Si_3N_4 and β-Si_3N_4. In the following figures, we presented the calculation results starting by:

1. The alpha phase

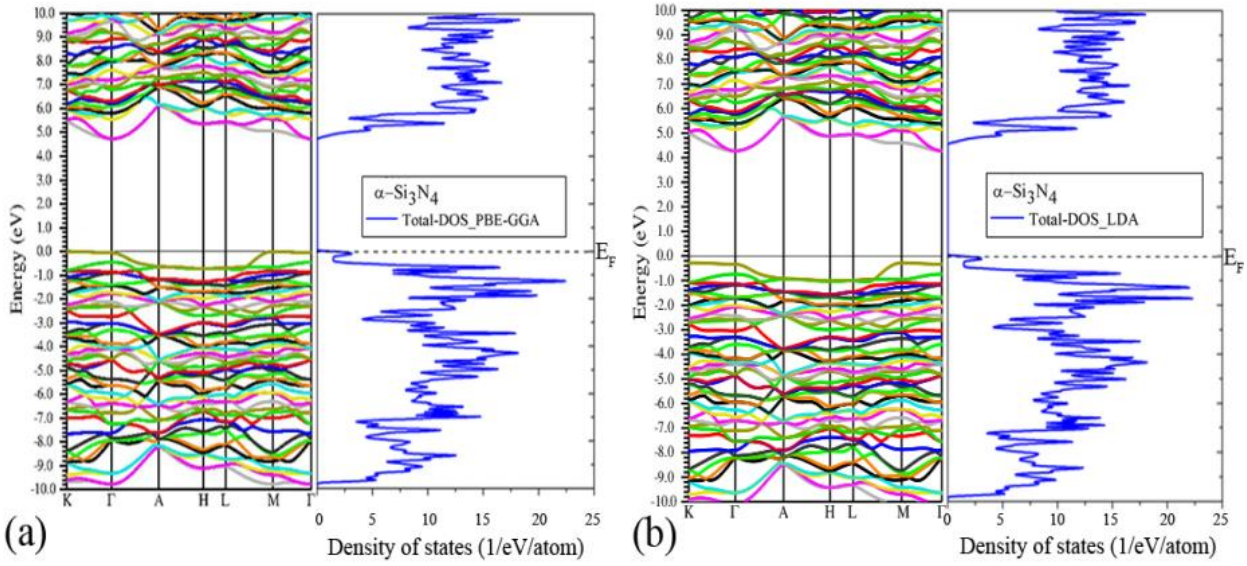

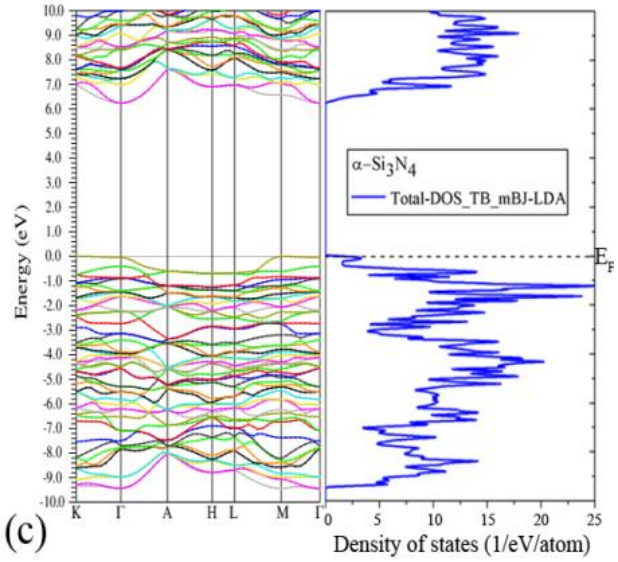

Figure III.4: *Band structures and total DOS for* α-Si_3N_4 *obtained by (a) PBE-GGA (b) LDA (c) TB-mBJ-LDA.*

Fig III.4 shows the band structures and the corresponding total DOS for α-Si_3N_4 according to PBE-GGA, LDA and TB-mBJ-LDA approximations. In each of these three approximations, we can see that the maximum of valence band is at Γ point and the minimum of the conduction band is also at the Γ point, so the phase α-Si_3N_4 is a semiconductor with direct bandgap. In the Tab III.2, we present the values of band gap for each approach and experimental value of other work.

	PBE-GGA	LDA	TB-mBJ-LDA	Experimental [3]
α-Si_3N_4 Bandgap (eV)	4.57	4.38	6.09	5.0

Table III.2: *Energy values of* α-Si_3N_4 *Bandgap.*

2. The beta phase

Now, we show the band structures and the DOS of beta phase. The results are obtained by the use of WC, PBE-GGA, LDA and TB-mBJ-LDA approximations.

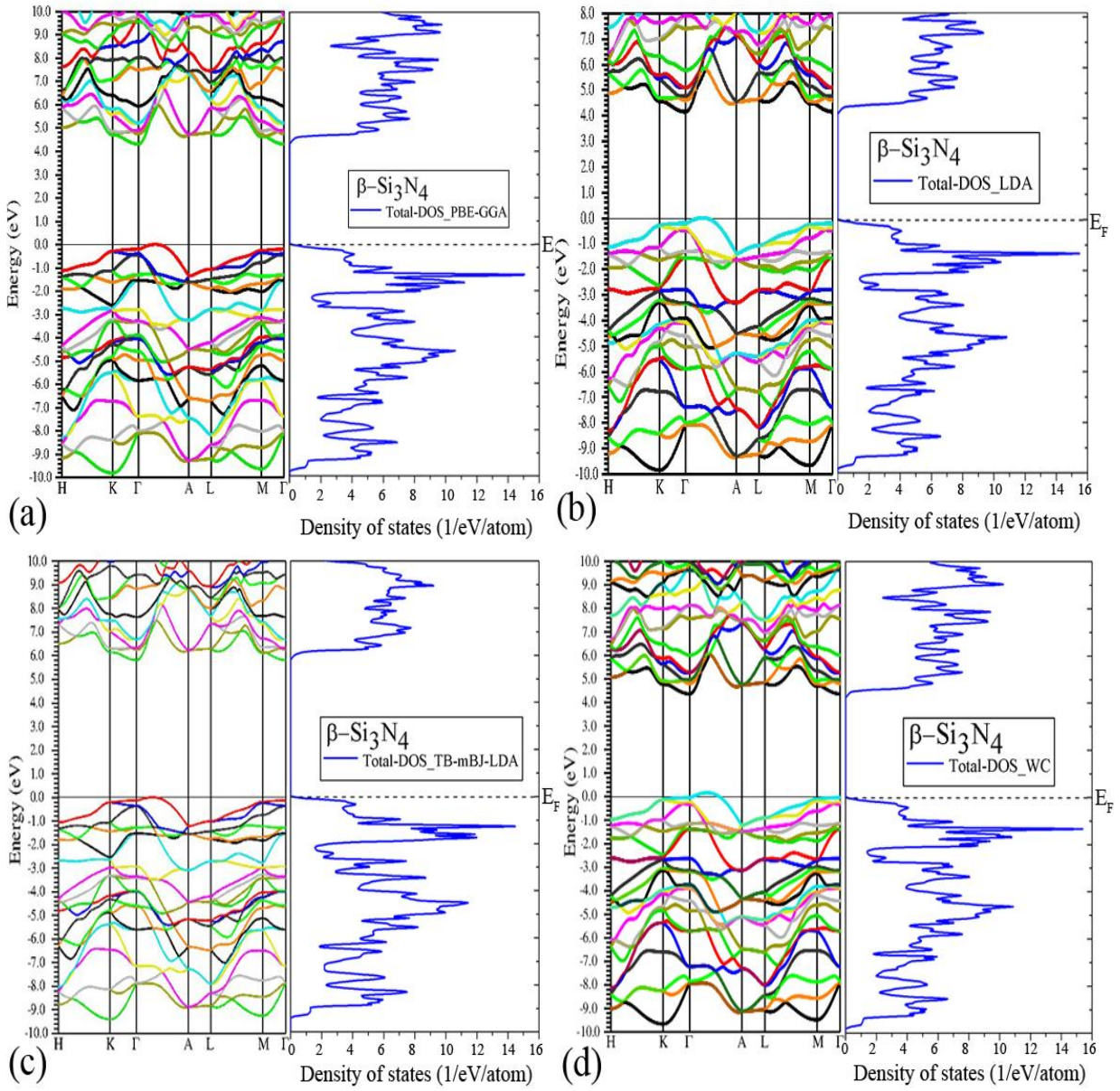

Figure III.5: *Band structures and total DOS for* β-Si_3N_4 *obtained by (a) PBE-GGA (b) LDA (c) TB-mBJ-LDA (d) WC.*

For the beta phase, we see that the maximum of the valence band is between Γ and A high-symmetry points while the maximum of the conduction band is at Γ point, so the β-Si_3N_4 phase has indirect bandgap. In Tab III.3, we present the values obtained of the beta bandgap.

	PBE-GGA	LDA	TB-mBJ-LDA	WC	Experimental [3]
β-Si_3N_4 Bandgap (eV)	4.13	4.0	5.65	4.05	4.6-5.5

Table III.3: *Energy values of* β-Si_3N_4 *Bandgap.*

From the Tab III.2 and Tab III.3 we observe that the β phase has the lowest bandgap compared with α phase.

III.4.2. Density of states

To understand the electronic properties, one must calculate the density of states, so in the following, we show the total and partial density of states of silicon nitride in their crystallographic phases α and β.

1. The alpha phase

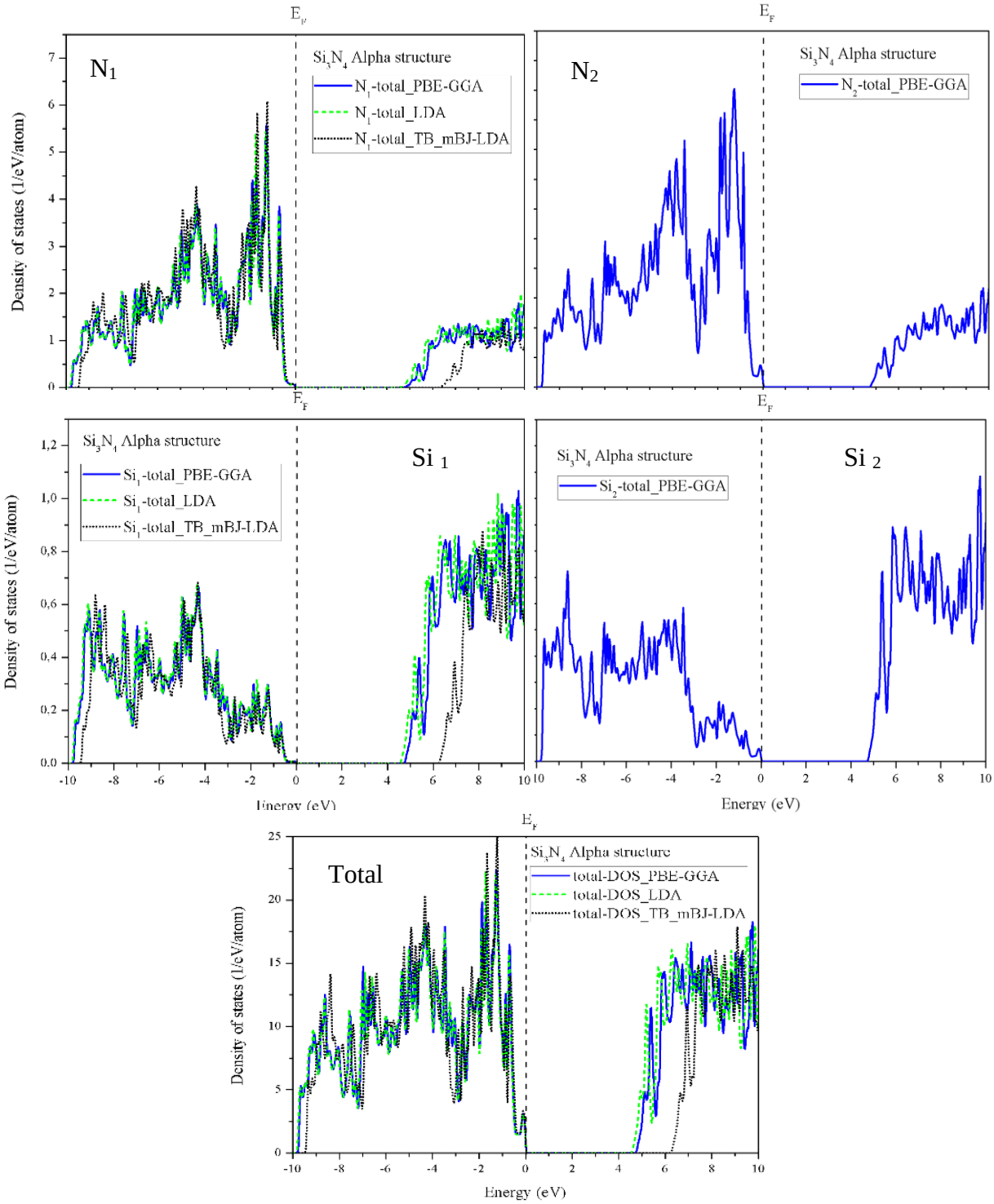

Figure III.6: *Total and partial density of states of alpha phase.*

2. The beta phase

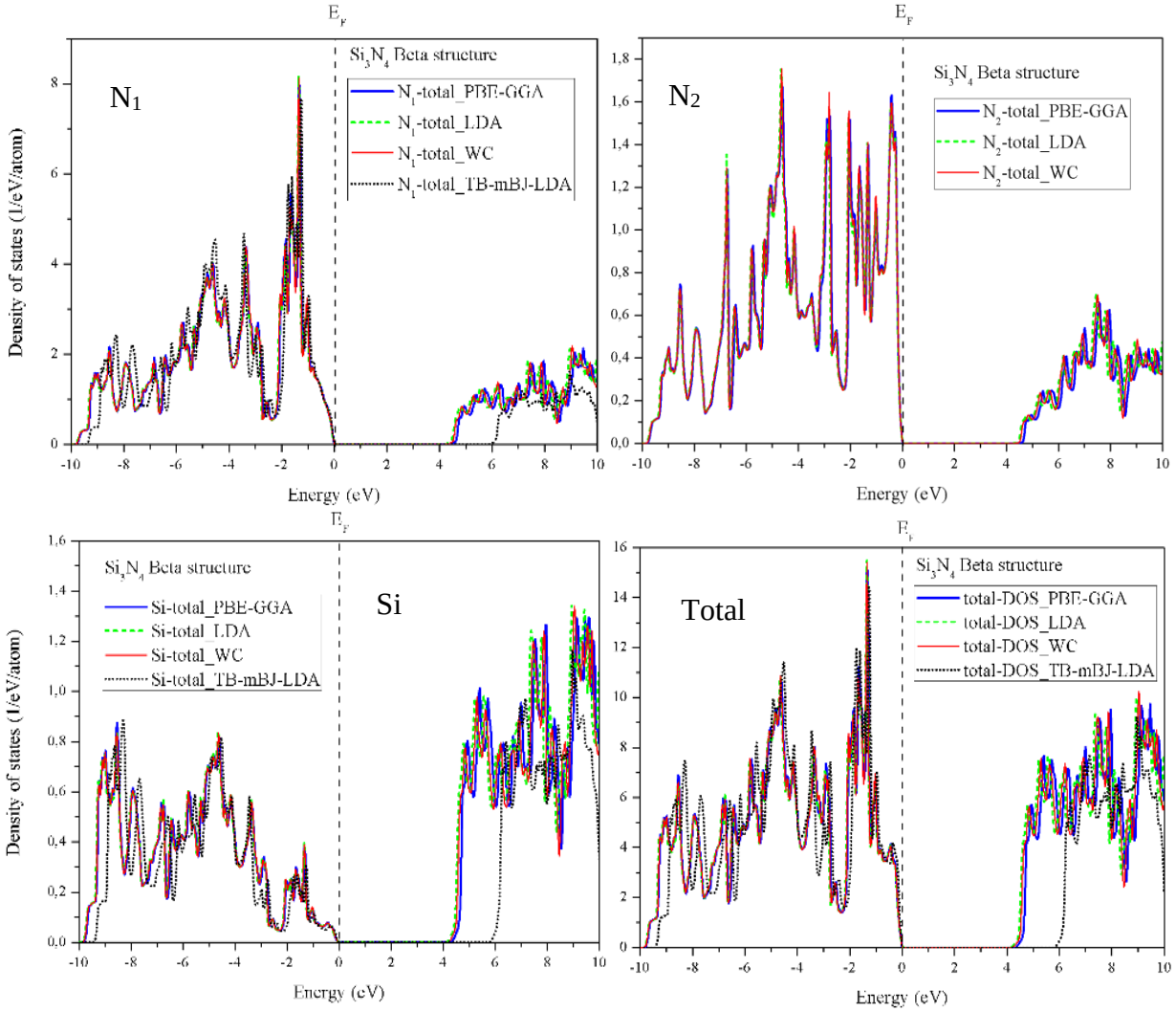

Figure III.7: *Total and partial density of states of beta phase.*

Fig III.6 shows the total DOS of α-Si_3N_4 phase and density of states of the atoms N_1, N_2, Si_1 and Si_2, the other atoms, by symmetry will be at the same state. In Fig III.7 we present the total DOS of β-Si_3N_4 phase and the DOS of N_1, N_2, and Si atoms. In both phases, the bottom of conduction bands is mainly constituted of Si 3s 3p states, and the top of valence bands is occupied by N 2p states [9].

Before the finish with the electronic properties part, we present in a comparative table the deduced properties for the two phases.

		PBE-GGA	LDA	TB-mBJ-LDA	WC
α	gap (eV)	4.57	4.38	6.09	-
	gap type	direct	direct	direct	-
	VB width (eV)	9.83	9.88	9.51	-
	CB width (eV)	5.34	5.52	3.82	-
β	gap (eV)	4.13	4.0	5.65	4.05
	gap type	indirect	indirect	indirect	indirect
	VB width (eV)	9.85	9.91	9.46	9.88
	CB width (eV)	5.76	5.91	4.26	5.84

Table III.4: *Electronic properties of Alpha and Beta phases.*

III.5. Optical properties

DFT makes it possible to calculate all the optical properties, namely the refractive index, the extinction coefficient, the absorption coefficient…, which are deduced from the complex dielectric function ε (ω).

III.5.1. Dielectric function

The optical properties of matter can be described by the complex dielectric function ε(ω), which represents the linear response of the system to an external electromagnetic field with a small wave vector. To calculate the direct inter-band contribution to the imaginary part of the dielectric function ε_2 (ω), one must sum all possible transitions from occupied to unoccupied states. The imaginary part ε_2 (ω) can be calculated by the following formula.

$$\varepsilon_2(\omega) = \frac{4\pi e^2}{m^2\omega}\int d^3k \sum_{n,n'} |\langle Kn|P|Kn'\rangle|^2 f_{Kn}(1 - f_{Kn'})\delta(E_{Kn} - E_{Kn'} - \hbar\omega) \qquad \text{(III. 1)}$$

Where e is the electron charge, m is the mass, ω is the frequency of the incident radiation, ħ is the reduced Planck constant, P the momentum operator, f_{Kn} the Fermi distribution and $|Kn'\rangle$ the crystal wave function [4].

We present by Fig III.8 and Fig III.9 the curves of the real part (ε_1) and the imaginary part (ε_2) of the dielectric function as a function of the photon energy.

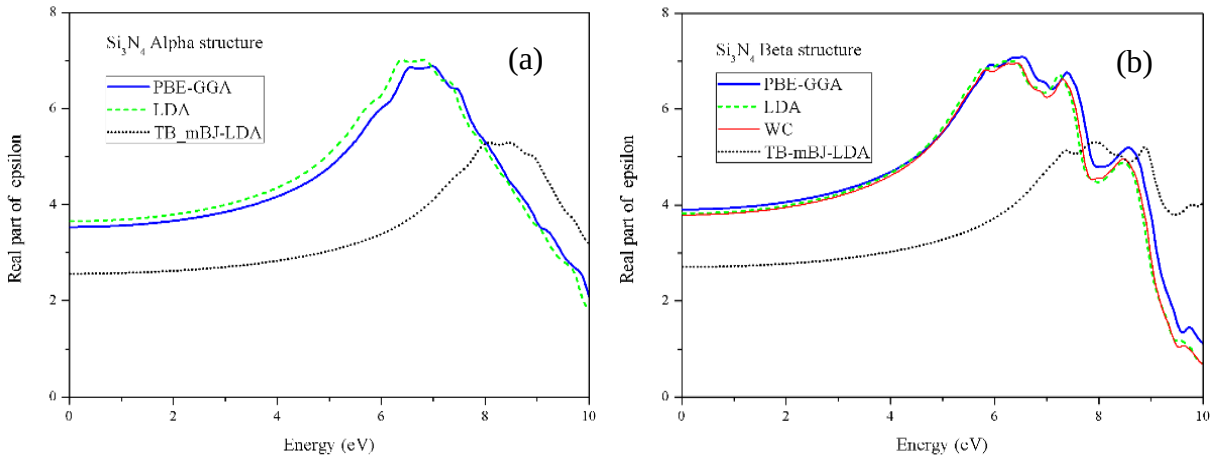

Figure III.8: *Variation of real part of the dielectric function for (a) α and (b) β phases.*

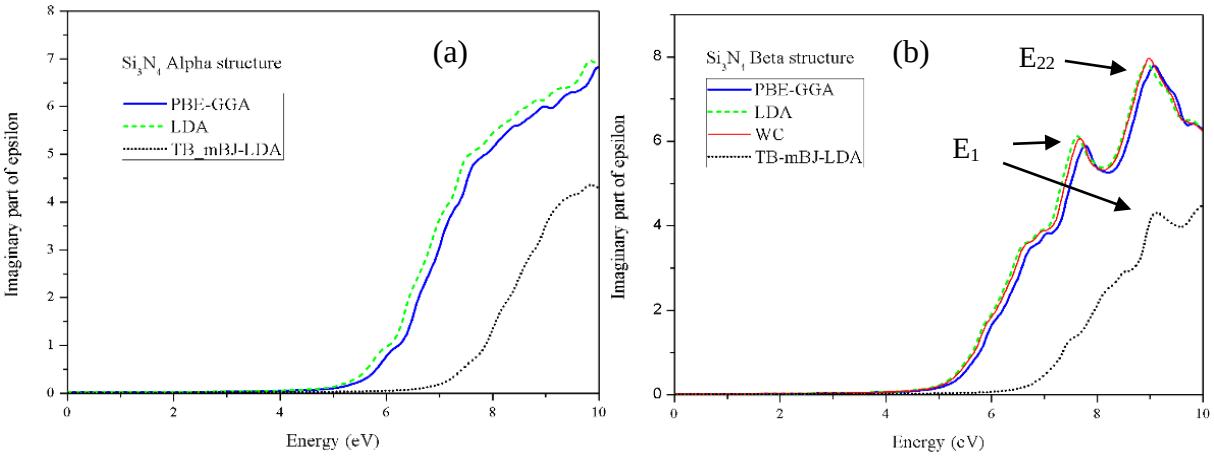

Figure III.9: *Variation of imaginary part of the dielectric function for (a) α and (b) β.*

The main feature of the real part (ε_1) in alpha phase is that the main peak appear approximately at the energy range [6, 7.5eV] obtained by PBE-GGA and LDA, and at [8, 9eV] for TB-mBJ-LDA approximation. For the beta phase, the peaks appeared at the energy range [5.8, 8eV] which obtained by the use of WC, PBE-GGA and LDA approximations, and at the range [7.3, 9eV] in the curve obtained by the TB-mBJ-LDA. These peaks are originating from the interband transition. In the Tab III.5 we present the static dielectric constants ε_1 (0) for both α and β phases.

		PBE-GGA	LDA	TB-mBJ-LDA	WC
α	ε_1 (0)	3.53	3.65	2.56	-
β	ε_1 (0)	3.90	3.82	2.70	3.79

Table III.5: *Calculated static dielectric constant ε_1 (0) for α and β phases.*

The Fig III.9 show the imaginary part (ε_2) of the dielectric function for alpha and beta phases. We observe two peaks E_1 and E_2, appeared in the beta phase correspond to the interband transitions. The positions of the two peaks are summarized in Tab III.6.

	PBE-GGA	LDA	WC	TB-mBJ-LDA
E_1 (eV)	7.76	7.63	7.68	9.12
E_2 (eV)	9.07	8.93	8.99	-

Table III.6: *Inter-band transition energies for β phase.*

III.5.2. Refractive index and extinction coefficient

The refractive index n (ω) and the extinction coefficient k (ω), are calculated in terms of the real and the imaginary parts of the complex dielectric function as follows [4]:

$$n = \frac{\left(\varepsilon_1 + (\varepsilon_1^2 + \varepsilon_2^2)^{1/2}\right)^{1/2}}{\sqrt{2}} \qquad \text{(III. 2)}$$

$$k = \frac{\left(-\varepsilon_1 + (\varepsilon_1^2 + \varepsilon_2^2)^{1/2}\right)^{1/2}}{\sqrt{2}} \qquad \text{(III. 3)}$$

The refractive index n (ω) and the extinction coefficient k (ω) of α and β phases are shown in Fig III.10 and Fig III.11 respectively.

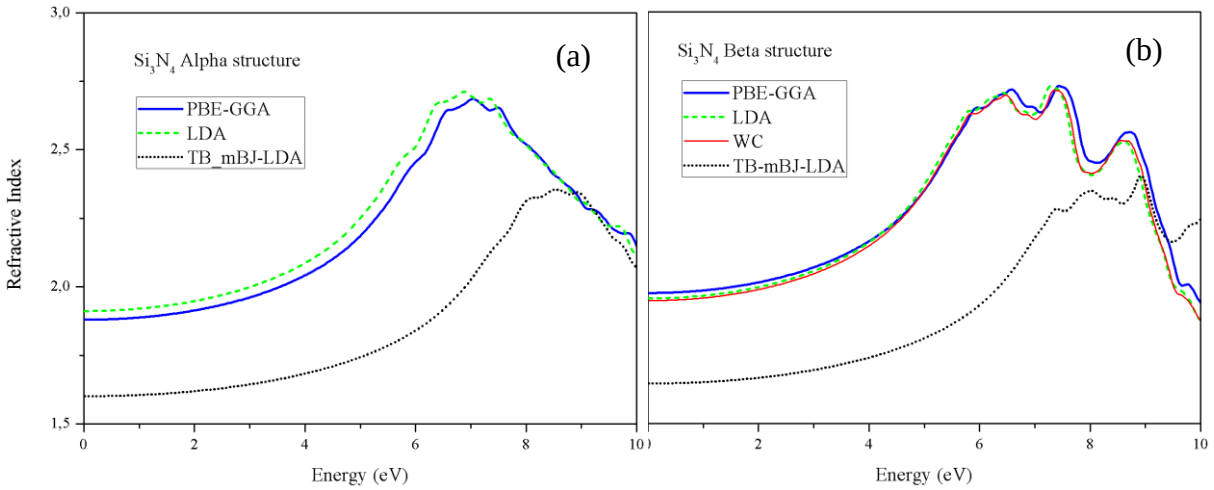

Figure III.10: *Variation of the refractive index for (a) α and (b) β phases.*

The spectra of refractive indices n (ω) of the two phases have similar frequency dependent features like ε_1 (ω) spectra. The Tab III.7 shows the static and maximum values of refractive index for α and β phases, obtained by each approximation.

		PBE-GGA	LDA	TB-mBJ-LDA	WC
α	n(0)	1.87	1.91	1.60	-
	n_{max} at E(eV)	n = 2.68 E = 7.03	n = 2.71 E = 6.87	n = 2.35 E = 8.53	-
β	n(0)	1.97	1.95	1.64	1.94
	n_{max} at E(eV)	n = 2.72 E = 7.44	n = 2.72 E = 7.27	n = 2.40 E = 8.91	n = 2.71 E = 7.36

Table III.7: *Static and maximum values of refractive index for α and β phases.*

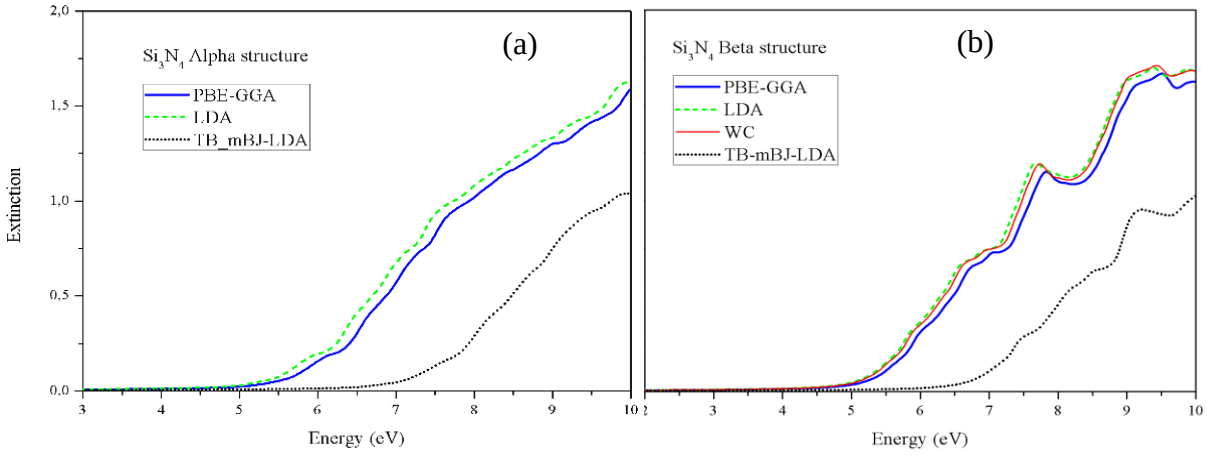

Figure III.11: *Variation of the extinction coefficient k (ω) for (a) α and (b) β phases.*

The imaginary part of the complex refractive index, namely extinction coefficient is known to be associated with ε_2 (ω). Therefore, change in photon frequency dependent ε_2 (ω) and change in photon frequency dependent extinction coefficient are shown similar behaviors. The extinction coefficient k (ω) vanishes for energies lower than 5 eV for both alpha and beta phases, and shows peaks in the beta phase due to the interband transitions in the energy ranges [7.5, 8eV] for PBE-GGA, LDA and WC approximations and [9, 10eV] for TB-mBJ-LDA. At values where extinction coefficient is high, it can be expected absorption coefficient to be high also, thus in this energy ranges the photons are absorbed rapidly.

III.5.3. Absorption coefficient and reflectivity

The absorption coefficient α (ω) can be written in the following form:

$$\alpha(\omega) = \frac{2k\omega}{c} \qquad \text{(III. 4)}$$

And the reflectivity R (ω) is written in the form:

$$R(\omega) = \frac{(n-1)^2 + k^2}{(n+1)^2 + k^2} \qquad \text{(III. 5)}$$

Where k is the extinction coefficient, ω is the frequency of the incident radiation, n is the index of refraction and c is the speed of light [5].

Fig III.12 shows the absorption coefficient α (ω) as a function of the energy of the incident photons.

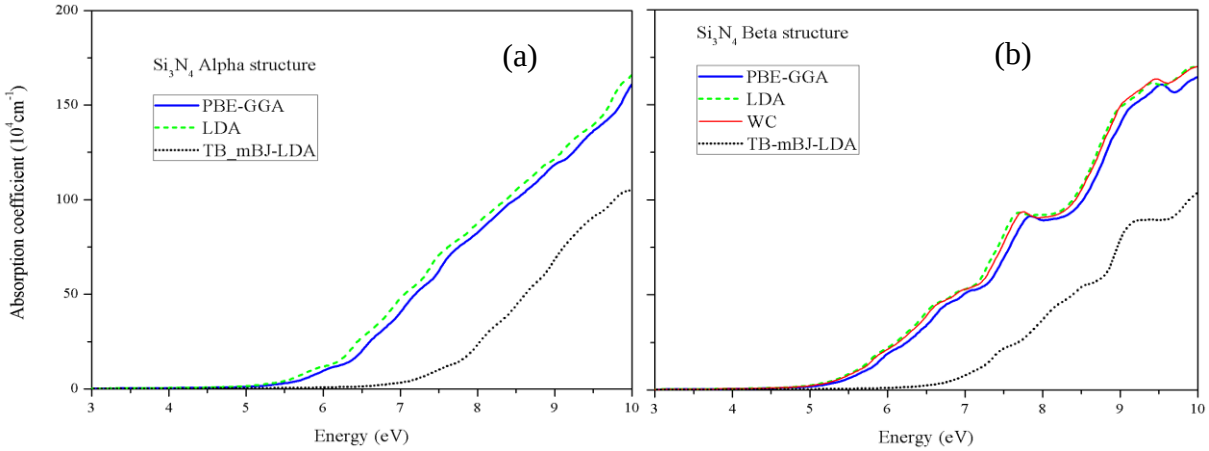

Figure III.12: *Variation of absorption coefficient α (ω) for (a) α and (b) β phases*.

By considering that the range of visible domain start from 380 nm to 740 nm, so the correspond photons energy range is from 1.67 eV to 3.26 eV, in this range, the absorption coefficient is almost zero in the two phases. But we see that the absorption coefficient of the two crystallographic phases of silicon nitride is highly in the ultraviolet range. As it appears in the graphs, the max of absorption coefficient is at E = 10 eV for both α and β phases, for the visible range, the maximum value is in the limit of range (3.25eV). In Tab III.8, the maximum values are summarized.

		PBE-GGA	LDA	TB-mBJ-LDA	WC
α	α (ω) (10^4.cm^{-1}) at E = 10 eV	161.08	166.07	105.36	-
	α (ω) (10^4.cm^{-1}) at E = 3.25 eV	0.291	0.312	0.157	-
β	α (ω) (10^4.cm^{-1}) at E = 10 eV	164.59	170.27	103.94	170.18
	α (ω) (10^4.cm^{-1}) at E = 3.25 eV	0.335	0.358	0.177	0.351

Table III.8: *Maximum values of absorption coefficient for α and β phases*.

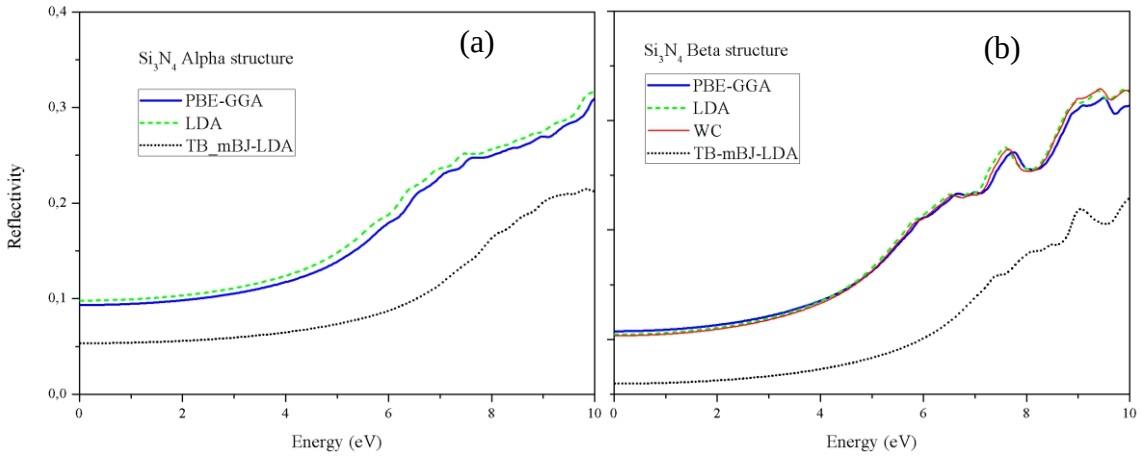

Figure III.13: *Variation of reflectivity R (ω) for (a) α and (b) β phases*.

The Fig III.13 shows that the maximum of reflectivity is at the energy E = 10 eV for the alpha phase and in the energy range [9.42, 10eV] for the beta phase. For the visible range, the maximum is at E = 3.25 eV for the both phases. In the Tab III.9, we summarize the maximum of reflectivity in the total energy range and in the visible range.

		PBE-GGA	LDA	TB-mBJ-LDA	WC
α	R(ω) (%) at E = 3.25 eV	10.78	11.36	6.05	-
	$R(\omega)_{max}$ (%)	30.96	31.73	21.47	-
β	R(ω) (%) at E = 3.25 eV	12.41	12.24	6.78	12.08
	$R(\omega)_{max}$ (%)	32.06	32.81	22.99	32.90

Table III.9: *Maximum values of reflectivity for α and β phases.*

III.5.4. Optical conductivity

The term of "optical conductivity" means the electrical conductivity in the presence of an alternating electric field [6]. The real part of optical conductivity is given by [7]:

$$Re[\sigma(\omega)] = \frac{\omega}{4\pi}\varepsilon_2(\omega) \qquad \text{(III. 6)}$$

The calculated optical conductivity is plotted in Fig III.14 for real part σ_1 (ω) and III.15 for imaginary part σ_2 (ω).

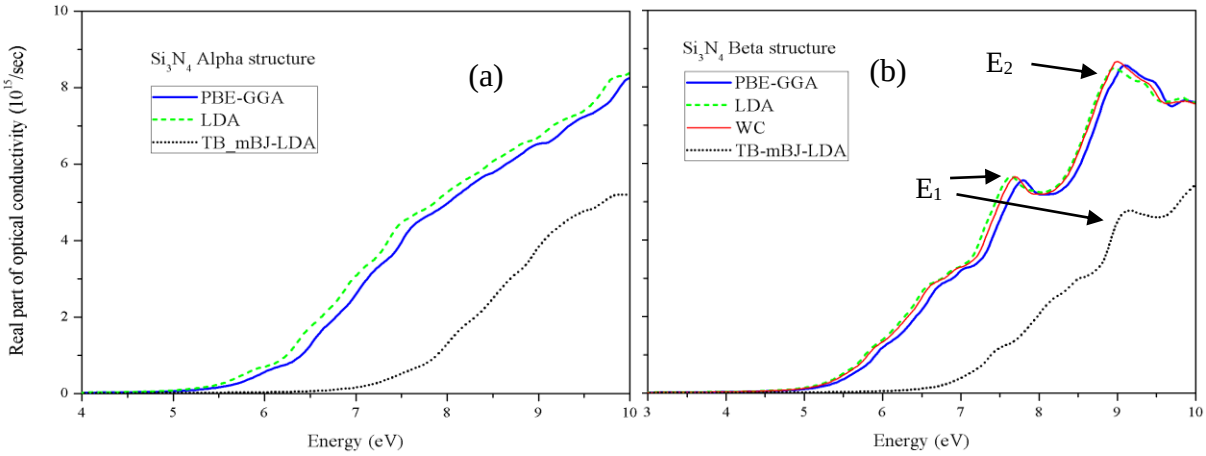

Figure III.14: *Real part of optical conductivity (10^{15}/sec) for (a) α and (b) β phases.*

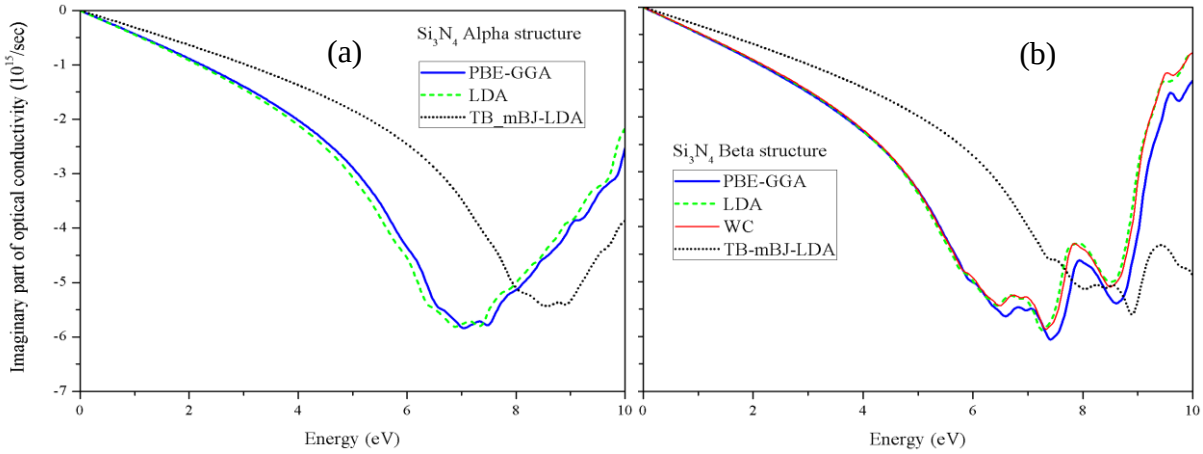

Figure III.15: *Imaginary part of optical conductivity (10^{15}/sec) for (a) α and (b) β phases.*

For the real part of optical conductivity, only in beta phase, peaks are appeared. This can be explained by the occupied states close to the conduction band minimum. Energies that correspond to these appeared peaks are summarized in Tab III.10. Also σ_1 (ω) have similar frequency dependent features like ε_2 (ω) spectra.

	PBE-GGA	LDA	WC	TB-mBJ-LDA
E_1 (eV)	7.79	7.63	7.68	9.15
E_2 (eV)	9.1	8.96	8.99	-

Table III.10: *Energies that correspond to optical conductivity peaks in the β phase.*

III.5.5. Energy loss function

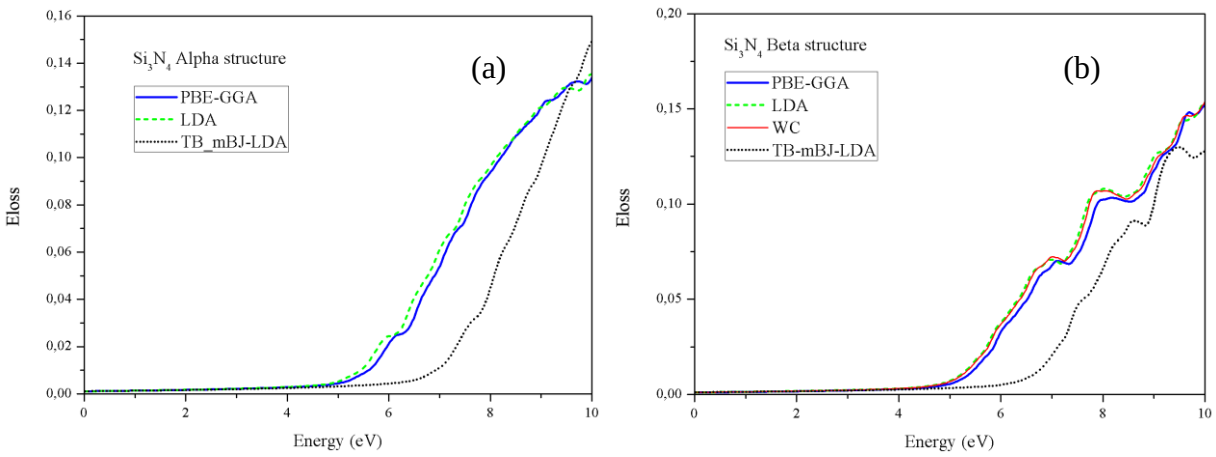

Figure III.16: *The energy loss function versus photon energy for (a) α and (b) β phases.*

Fig III.16 shows the energy loss function for the two phases, it is given by [8]:

$$L(\omega) = Im\left(\frac{-1}{\varepsilon(\omega)}\right) \qquad \text{(III. 7)}$$

The energy loss function is important for investigating the optical properties of materials; it covers the complete energy range, consisting of non-scattered and elastically scattered electrons, which are responsible for the interband transitions. When electrons of sufficient energy pass through the solid, the amount of energy lost when an electron jumps in the material is described by the loss function. The peaks in the energy loss function are related to interband transitions. As shown in Fig III.16, the energy loss function is negligible in both alpha and beta phases for the energies lower than 5 eV, and after this energy the energy loss function increase with the increase of the incident photon energy, until reaching their maximum in the energy range [9.5-10eV] for the both phases.

Through the analysis of the results obtained in each phase, we find that the properties of beta phase is relatively better than the properties of alpha phase, such as the absorption coefficient which is relatively higher (in the visible range) in beta phase compared to alpha phase.

III.6. Optimization of beta phase properties

As we mentioned before, we are studying the electronic and optical properties of silicon nitride in the crystallographic phases α and β, to use them as anti-reflective layers on mono- or multi-crystalline silicon-based solar cells. For this, one must choose the crystallographic phase, which has characteristics more suitable for this type of applications. So after we studied the properties of both phases, we find that the beta structure is suitable film crystallization. However, their properties in the visible range remain very weak, so we will resort to improve it by doping with aluminum (Al) for obtaining the p-type conductivity, and with phosphorus (P) for obtaining n-type conductivity. The results allow us to conclude with respect to the study need to separate between both elements.

The unit cell of the beta phase contains 6 atoms of (Si), and the doping is done by the use of one atom of (P) instead of the atom of (Si) in the first case, so we have 16.66% of (P) and 83.33% of (Si), and the same for the doping with atom of (Al), so we obtain the compounds P-doped β-$(Si_{0.83}P_{0.16})_3N_4$ and Al-doped β-$(Si_{0.83}Al_{0.16})_3N_4$.

Taking the electronic configuration of atoms: P: $1s^2 2s^2 2p^6 3s^2 3p^3$ Al: $1s^2 2s^2 2p^6 3s^2 3p^1$

III.6.1. Novel electronic properties of β-Si_3N_4 with Al and P dopants

A better evaluation of the electronic properties is made by using the TB-mBJ-LDA, so we've used it in the remaining calculation.

III.6.1.1. Band structures

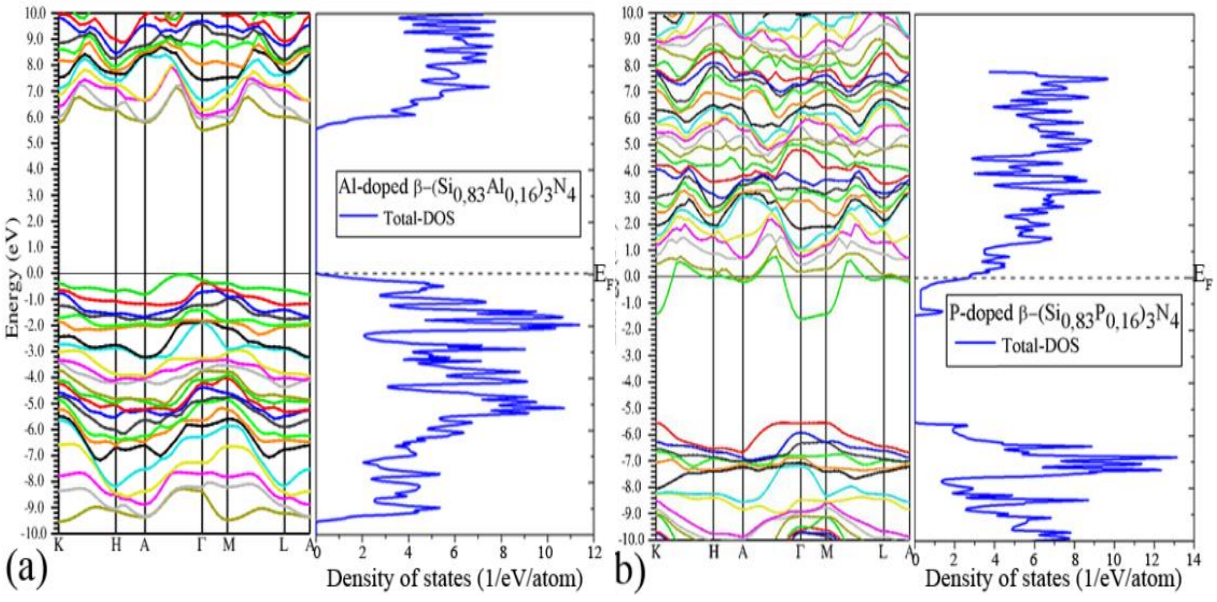

Figure III.17: *Band structures and total DOS of (a) Al and (b) P doped β-Si_3N_4.*

In the Tab III.11, we present the values obtained for the two elements compared with the undoped beta structure.

	Gap (eV)	Gap type	VB width (eV)	CB width (eV)
P-doped β-Si_3N_4	4.02	direct	6.03	9.93
Al-doped β-Si_3N_4	5.46	indirect	9.63	4.46
Undoped β-Si_3N_4	5.65	indirect	9.46	4.26

Table III.11: *Band gap comparison between doped and undoped β phase.*

We see that the gap has become direct and decreases from 5.65 eV to 4.02 eV in P-doped, it's a remarkable improvement compared with the obtained in Al-doped where the gap decreases from 5.65 eV to 5.46 eV and remain indirect gap. On the other hand, the width of the VB and the CB of Al-doped β-Si_3N_4 not much different from the width of VB and CB of the undoped beta phase compared with the VB and the CB of P-doped β-Si_3N_4, where the width of VB decreases from 9.46 eV to 6.03 eV and the width of CB increases from 4.26 eV to 9.93eV. This is because the P atom has one more conduction electron than Si atom which acts as a donor when it replaces the Si atom.

III.6.1.2. Density of states

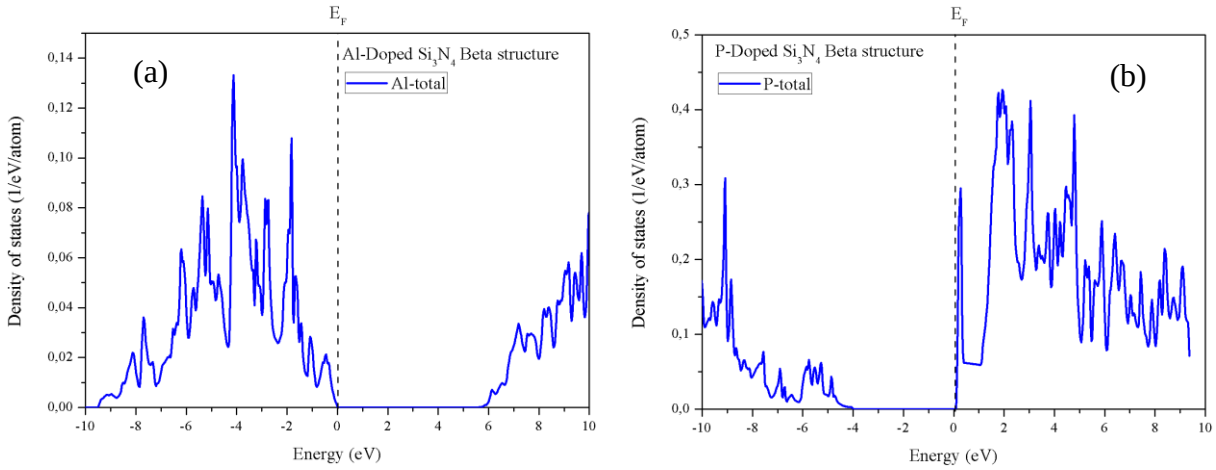

Figure III.18: *Total density of states for (a) Al and (b) P atoms.*

One can observe that the Al atom has more states in the valence band and less states in the conduction band, and the inverse for the P atom. This is because the Al atom has a vacant position and acts as an acceptor when it replaces the Si atom, and the P atom has one more conduction electron than Si atom which acts as a donor. So, Al (3p) and N (2p) states occupy the top of valence band of Al-doped β-Si_3N_4. The bottom of conduction bands is mainly constituted of Si (3s; 3p). The top of valence band of P-doped β-Si_3N_4 is occupied by N (2p)

states, and the conduction band consists mainly by the contribution of P (3s; 3p) and Si (3s; 3p) states [9].

While the Al-doped β-Si_3N_4 is a p-type semiconductor, so there are more holes in the valence band than there are electrons in the conduction band i.e. n < p. This implies that the probability of finding an electron near the conduction band edge is smaller than the probability of finding a hole at the valence band edge. Therefore, the Fermi level is closer to the valence band. On the other hand, the P-doped β-Si_3N_4 is an n-type semiconductor thus the Fermi level will shift towards conduction band.

III.6.2. Novel optical properties of β-Si_3N_4 with Al and P dopants

III.6.2.1. Dielectric function

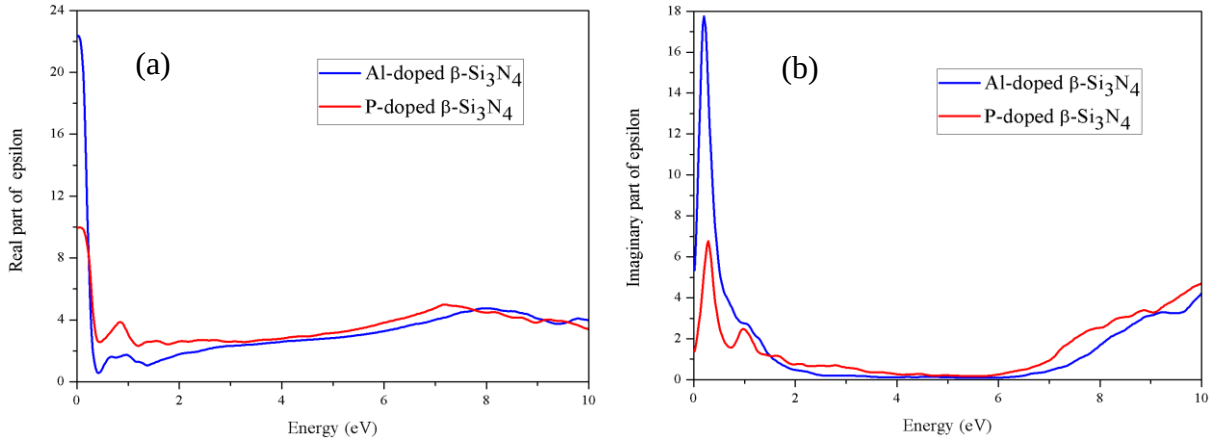

Figure III.19: *Variation of (a) real and (b) imaginary parts of the dielectric function for Al and P doped β-Si_3N_4.*

Fig III.19 shows the changes in photon energy dependent real and imaginary parts of dielectric functions after adding Al and P impurities to β-Si_3N_4 structure. When we see the imaginary part of the dielectric function in the two compounds, we find that there are values in the range [0, 6eV] compared with the undoped β structure, which is negligible in this energy range. Also, peaks are appeared at the energy range [0, 1eV] in the two compounds with the value of 6.76 for the max peak of P-doped β-Si_3N_4, and 17.75 for Al-doped β-Si_3N_4, it mean that the interband transition occur in low energy. On the other hand, we observe a decrease in ε_2 at the range [6, 10 eV] for both compounds compared with the undoped β structure. For the real part ε_1, the maximum is the static value ε_1 (0), it is 9.97 for P-doped β-Si_3N_4, and 22.36 for Al-doped β-Si_3N_4.

III.6.2.2. Refractive index and extinction coefficient

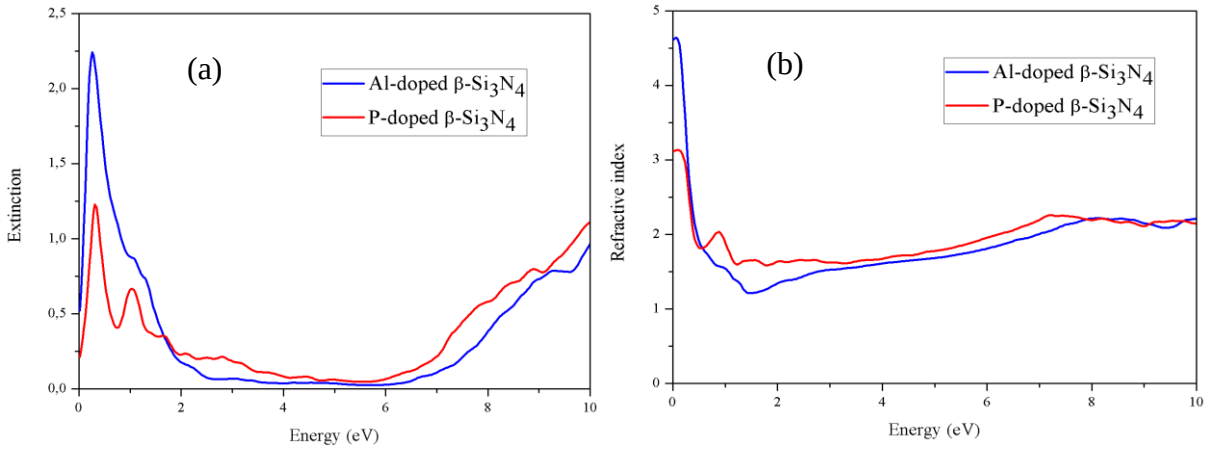

Figure III.20: *Variation of (a) extinction coefficient k (ω) and (b) refractive index for Al and P doped β-Si_3N_4.*

The change in the refractive index is proportion to the change in ε_1 (ω) .We see that the maximum of refractive index had become the static value n (0), it is 3.11 for P-doped β-Si_3N_4 and 4.61 for Al-doped β-Si_3N_4, where the static value of the undoped β structure was 1.64 and the maximum value is 2.40 at the energy E = 8.91eV (obtained by TB-mBJ-LDA).

Since the extinction coefficient is associated with ε_2 (ω), so its change have similar behaviors of the change in the ε_2 (ω). For that, we see that the extinction coefficient have values for the energies lower than 5 eV, and the maximum of k (ω) take place in the range [0, 1eV] for both Al and P doped β-Si_3N_4 and the max value is for Al-doped β-Si_3N_4, but in the visible range the values of P-doped β-Si_3N_4 is the highest.

III.6.2.3. Absorption coefficient and reflectivity

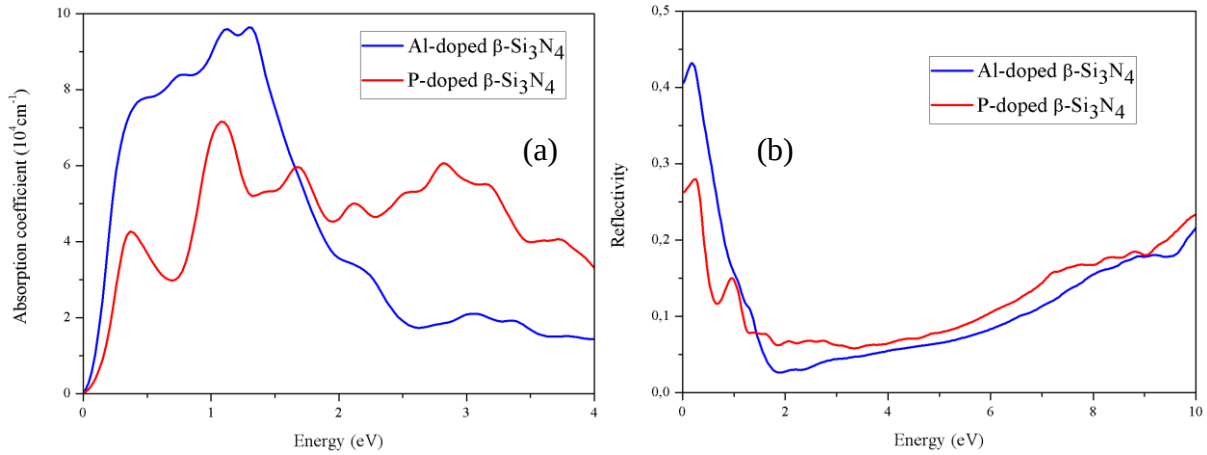

Figure III.21: *Variation of (a) absorption coefficient α (ω) and (b) reflectivity R (ω) for Al and P doped β-Si_3N_4.*

Compared with the undoped β-Si_3N_4 where the absorption coefficient almost zero in the visible range, the Al-doped β-Si_3N_4, and the P-doped β-Si_3N_4 showed a consider absorption coefficient in the visible range. In the following table, we present values and positions of the maximum absorption coefficient in the visible range [1.67, 3.26eV] for the two compounds compared with the undoped β-Si_3N_4. We see that the P-doped β-Si_3N_4 is better light absorber than the Al-doped β-Si_3N_4.

	α (ω) (10^4.cm^{-1})	at E (eV)
P-doped β-Si_3N_4	6.06	2.81
Al-doped β-Si_3N_4	5.80	1.67
Undoped β-Si_3N_4	0.177	3.25

Table III.12: *Maximum values of absorption coefficient in the visible range for Al and P doped β-Si_3N_4.*

For the reflectivity, we see that the maximum has become in the range [0, 1eV] instead of 10 eV, also we see peaks in this range, one peak in Al-doped β-Si_3N_4 and two peaks in P-doped β-Si_3N_4. The max of reflectivity is presented in the following table.

	R (ω) $_{max}$ (%)	R (ω) $_{max}$ (%) (visible range)
P-doped β-Si_3N_4	27.98	7.38
Al-doped β-Si_3N_4	43.16	4.57
Undoped β-Si_3N_4	22.99	6.78

Table III.13: *Maximum values of reflectivity for Al and P doped β-Si_3N_4.*

III.6.2.4. Optical conductivity

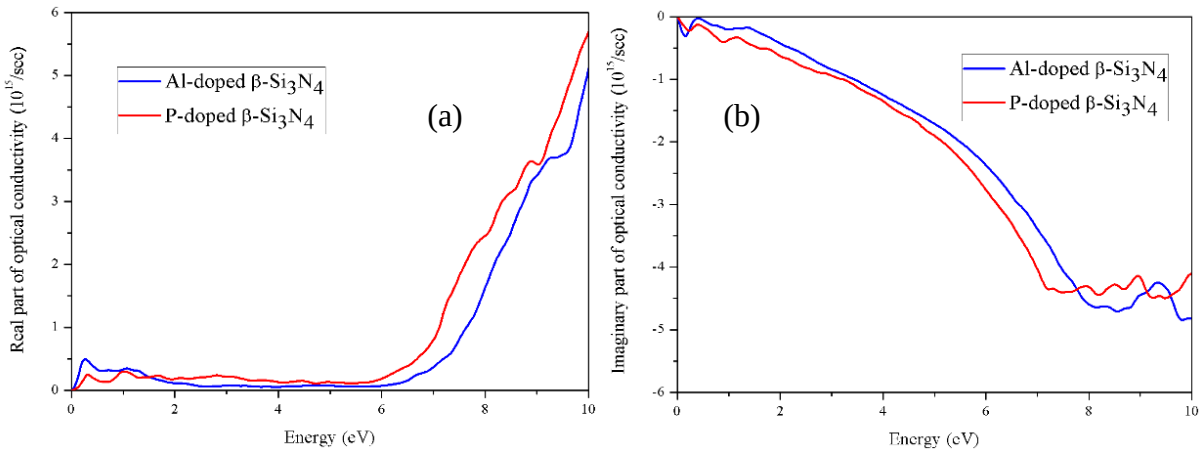

Figure III.22: *Variation of (a) Real and (b) imaginary parts of optical conductivity for Al and P doped β-Si_3N_4.*

Before doping the beta phase, the real part of optical conductivity was null in the range [0, 6eV], now there are values and it higher in the P-doped β-Si_3N_4 compared with Al-doped β-Si_3N_4.

III.6.2.5. Energy loss function

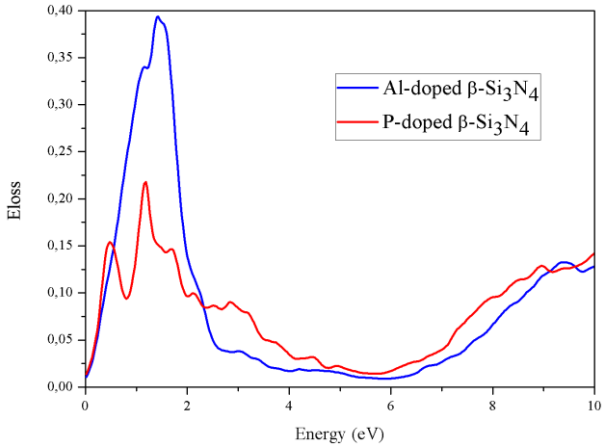

Figure III.23: *Variation of the energy loss function for Al and P doped β-Si_3N_4.*

Before doping the beta phase, the energy loss function was negligible in the range [0, 5eV]. Now, the highest loss in energy is in this range for the two compounds, where peaks are appeared at the range [0, 2eV], this means that an interband transition occurred in this energy range, also we see that the higher peak is for the Al-doped β-Si_3N_4 compound.

After seeing the novel electronic and optical properties of β-Si_3N_4 with Al and P dopants, we found that the P atom improved the properties more than the Al atom, especially the increase of the absorption coefficient in the visible range and the decrease of the bandgap. So we'll do another simulation for the P-doped β-Si_3N_4 with a change in the concentration of P, to see if we'll get more optimization by increasing the concentration. We will use 2 atoms of P beside 4 atoms of Si per unit cell, thus the concentration will be 33.33% of P and 66.66% of Si and so our compound becomes β-$(Si_{0.66}P_{0.33})_3N_4$.

III.6.3. Novel electronic properties of β-Si_3N_4 with P dopant

III.6.3.1. Band structure

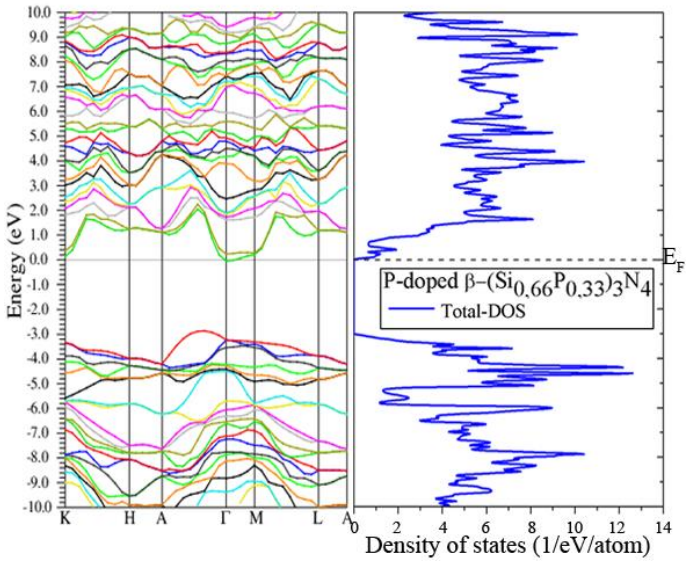

Figure III.24: *Band structure and total DOS for P-doped β-Si_3N_4 with new concentration.*

We see that the band gap decreases with the increase in the concentration of P. Tab III.14 below shows the change in the band structure of P-doped β-Si_3N_4 with the new concentration.

	Gap (eV)	Gap type	VB width (eV)	CB width (eV)
β-$(Si_{0.66}P_{0.33})_3N_4$	3.01	indirect	7.02	9.96
β-$(Si_{0.83}P_{0.16})_3N_4$	4.02	direct	6.03	9.93

Table III.14: *Band gap of P-doped β-Si_3N_4 with the two concentration.*

III.6.3.2. Density of states

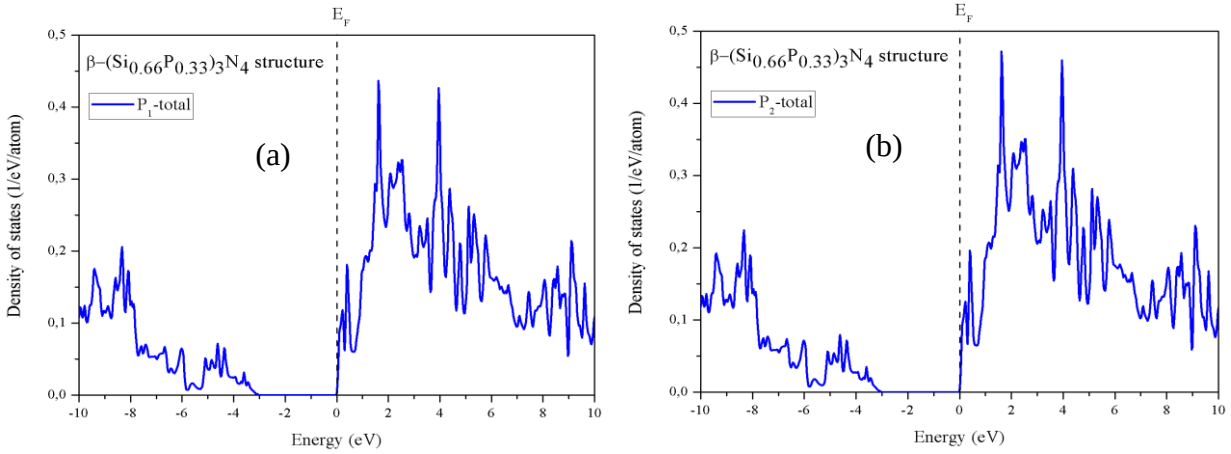

Figure III.25: *Density of states of phosphorus atoms, (a) P_1 and (b) P_2.*

Fig III.25 shows the density of states for the phosphorus atoms P_1 and P_2 of the β-$(Si_{0.66}P_{0.33})_3N_4$ compound. The contribution of two atoms of P in the total DOS leads to an increase in states of the whole structure.

III.6.4. Novel optical properties of β-Si_3N_4 with P dopant

III.6.4.1. Dielectric function

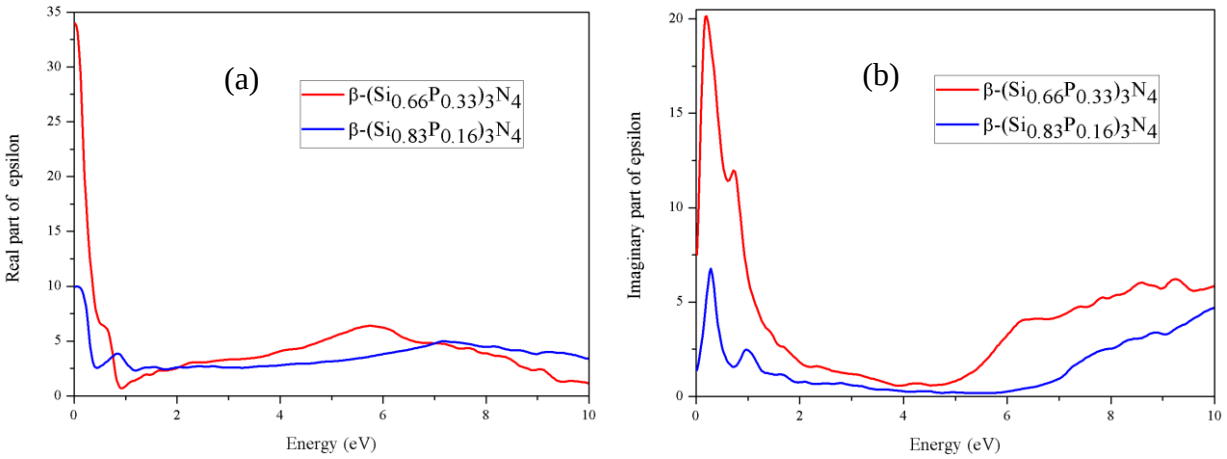

Figure III.26: *Variation of (a) real and (b) imaginary parts of the dielectric function for P doped β-Si_3N_4 with the two concentrations*.

From the Fig III.26, we can see that the increase in concentration of P leads to increase in the values of the dielectric function. For the real part (ε_1), the maximum value stay the static value ε_1 (0) but increase from 9.97 to 33.97, and for the imaginary part (ε_2), the value of the main peak increase from 6.76 to 20.13.

III.6.4.2. Refractive index and extinction coefficient

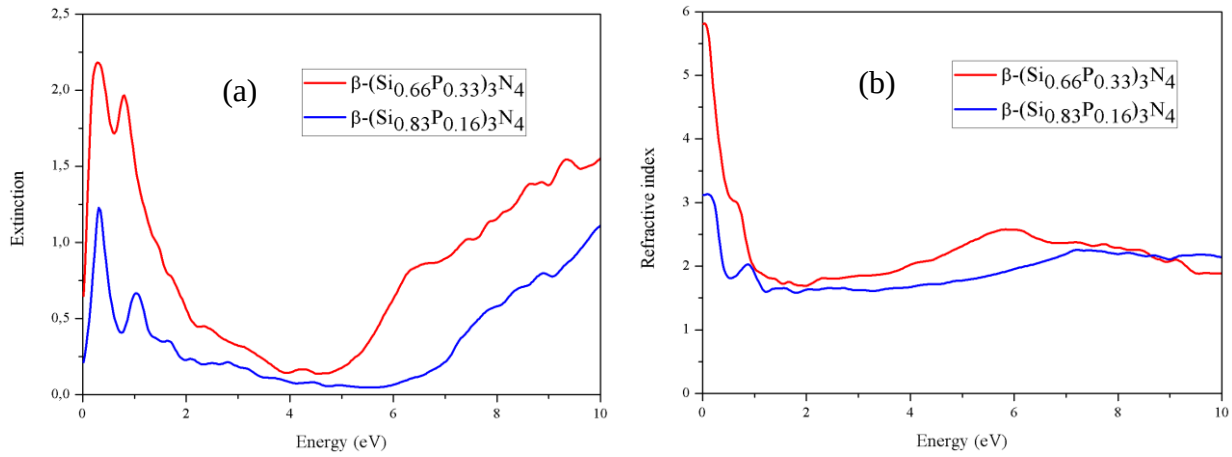

Figure III.27: *Variation of (a) extinction coefficient k (ω) and (b) refractive index for P doped β-Si3N4 with the two concentrations.*

We have noticed an increase in the refractive index value with the new concentration of P, the maximum become 5.81 instead of 3.11. Also, we have observed an increase in the extinction coefficient on all the range with the new concentration.

III.6.4.3. Absorption coefficient and reflectivity

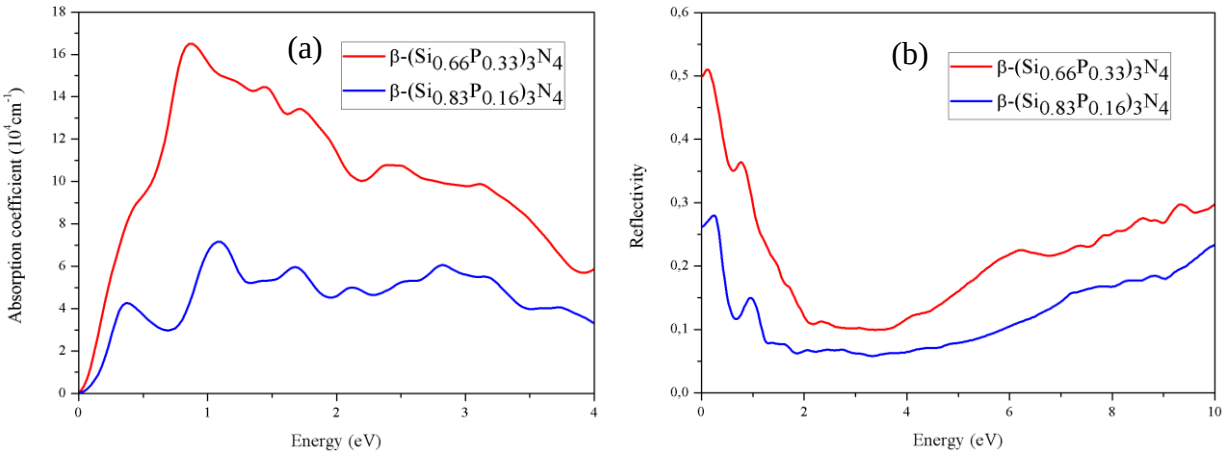

Figure III.28: *Variation of (a) absorption coefficient α (ω) and (b) reflectivity R (ω) for P doped β-Si3N4 with the two concentrations.*

Through the Fig III.28, we see that the increase in the concentration of P leads to a significant increment in the absorption coefficient and the reflectivity. The maximum of absorption coefficient in the visible range become 13.42 (10^4.cm^{-1}) instead of 6.06 (10^4.cm^{-1}). For the reflectivity, the maximum in the visible range become 16.89% instead of 7.38% and the maximum in the whole range become 51.02% instead of 27.98%.

III.6.4.4. Optical conductivity

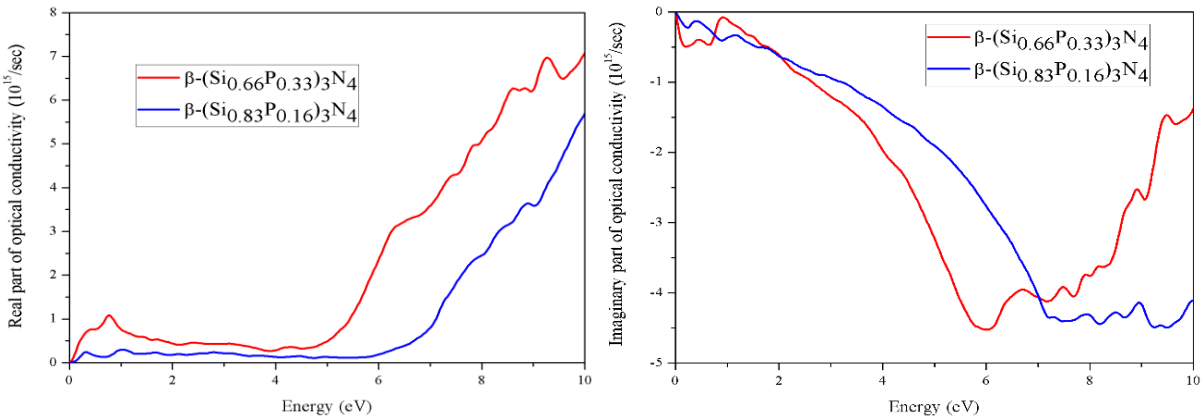

Figure III.29: *Variation of (a) Real and (b) imaginary parts of optical conductivity for P doped β-Si_3N_4 with the two concentrations.*

From Fig III.29, we can see that the optical conductivity increase with the increase in the P concentration especially in the visible range.

III.6.4.5. Energy loss function

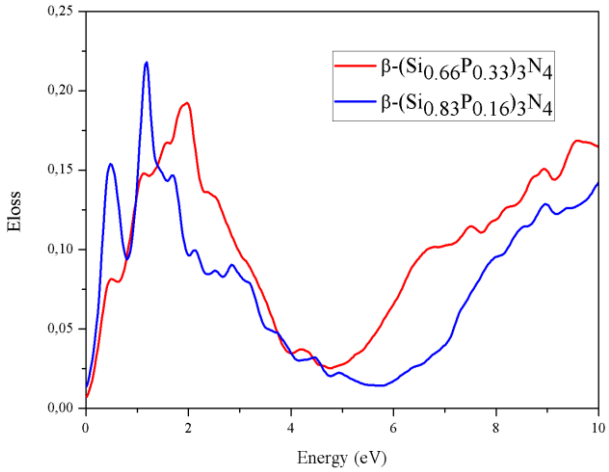

Figure III.30: *Variation of the energy loss function for P doped β-Si3N4 with the two concentrations.*

With the new concentration of P, the main peak of the energy loss function becomes in the visible range (at the energy 1.97eV instead of 1.18eV) because the interband transition occurred in this energy range, and from the energy (1.4eV) the energy loss function become higher compared with the first concentration.

In summary, the results have shown that the phosphorus atom gave more optimization to the properties of beta phase compared with the aluminum atom. In addition, we note that the increase in the phosphorus concentration leads to an increase in the absorption coefficient and in general, the optical properties.

Conclusion

Conclusion

In this work, we have done a systematic study based on density functional theory (DFT). We used the linearized augmented plane wave method (FP-LAPW) to calculate the electronic and optical properties of silicon nitride (Si3N4) in the crystallographic phases α and β. Besides, we have employed the PBE-GGA, LDA, WC and TB-mBJ-LDA approximations.

We have shown the electronic behavior of silicon nitride in both phases calculating for this issue the band structure and the density of states. The optical properties were calculated using the Kramers-Kronig dispersion relationship and we have determined all optical properties needed in an energy range extended to 10 eV, so that the dielectric tensor, the absorption coefficients, the refractive indices, and the conductivity, spectra are well presented.

The results of study showed that properties of beta phase are the suitable for the photovoltaic application and as an anti-reflective layer than the alpha phase, which present a higher absorption coefficient, as well as the others optical properties are also relatively better. However, their properties remain very weak in the visible range for what we have resorted to dope it with a point of view to improve its physical properties and making it more suitable for the photovoltaic application. We have used the aluminum (Al) and the phosphorus (P) as dopants. So, the calculation exhibits interested result with P-doped Si_3N_4 leading to the increase of the absorption coefficient and, in general, the optical properties more than with Al-doped Si_3N_4. Therefore, we increased the concentration of P to 33% in view to see the optical behavior, the calculation shown an optimization in the electronic properties, an increase in the absorption coefficient and the others optical properties yielding to get an important spectral response in visible range, which is the needed subject.

Finally, this study led to the understanding of the electronic and optical properties of the two phases of the silicon nitride, so this enables us to exploit it in several domains of applications such as anti-reflective layers, optoelectronic, photovoltaic and many other applications.

References

Introduction:

[1] Richard H. Bube, Photovoltaic Materials, Imperial College Press, (1998), p. vii.

[2] Donald A. Neamen, Semiconductor Physics and Devices Basic Principles 3rd edition, McGraw-Hill, (2003), p. 1.

[3] F. de Brito Mota, J.F. Justo and A. Fazzio, Structural properties of amorphous silicon nitride, Physical Review B, Vol 58, 13 (1998) p 8323-8328, https://doi.org/10.1103/PhysRevB.58.8323.

Chapter I:

[1] H. Eschrig, The Fundamentals of Density Functional Theory revised and extended version (2003), p. 9.

[2] John M.Wills, Mebarek Alouani, Per Andersson, Anna Delin, Olle Eriksson, Oleksiy Grechnyev, Full-Potential Electronic Structure Method, Springer, (2010), p. 7-18, https://doi.org/10.1007/978-3-642-15144-6.

[3] J.M. Seminario, Recent Developments and Applications of Modem Density Functional Theory 1st edition, Elsevier Science B.V. (1996) p. 3.

[4] Eberhard.Engel, Reiner M. Dreizler, Density Functional Theory an Advanced Course, Springer (2011) p. 5-6, https://doi.org/10.1007/978-3-642-14090-7.

[5] Wolfram Koch, Max C. Holthausen, A Chemist's Guide to Density Functional Theory 2nd edition, Wiley-VCH (2001) p. 5, 65, 70-71.

[6] David S. Sholl, Janice A. Steckel, Density Functional Theory a Practical Introduction, Wiley, (2009), p. 11, 15, https://doi.org/10.1002/9780470447710.

[7] Stefaan Cottenier, Density Functional Theory and the Family of (L) APW-methods: a step-by-step introduction 2nd edition, (2013) p. 4-7, 15-16, 21-22.

[8] Peter Blaha, Karlheinz Schwarz, Georg K. H. Madsen, Dieter Kvasnicka, Joachim Luitz, Robert Laskowski, Fabien Tran, Laurence D. Marks, WIEN2k An Augmented PlaneWave + Local Orbitals Program for Calculating Crystal Properties, User's Guide, WIEN2k 18.2 (2018), p. 18-20, 179-200.

[9] J.C. Slater, Wave Functions in a Periodic Potential, Phys Rev, Vol 51, (1937) p. 846-851, https://doi.org/10.1103/PhysRev.51.846.

[10] K. Schwarz, P. Blaha, G.K.H.Madsen, Electronic structure calculations of solids using the WIEN2k package for material sciences, Computer Physics Communications, 147, (2002), P. 71–76, https://doi.org/10.1016/S0010-4655(02)00206-0.

[11] D. R Hamann, Semiconductor Charge Densities with Hard-Core and Soft-Core Pseudopotentials, Phys. Rev. Lett, Vol 42, N° 10, (1979), p. 662-665, https://doi.org/10.1103/PhysRevLett.42.662.

Chapter II:

[1] Thomas Ihn, semiconductors Nanostructures Quantum States and Electronic Transport, Oxford University, (2010), p. 19.

[2] Marius Grundmann, The Physics of Semiconductors, springer, (2006), p. 111-113, 131, 145, 190-191, 627, https://doi.org/10.1007/978-3-319-23880-7.

[3] Jasprit Singh, Electronic and Optoelectronic Properties of Semiconductor Structures, Cambridge University press, (2003), p. 47.

[4] Chihiro Hamaguchi, Basic Semiconductor Physic, 2nd edition, springer, (2010), p. 13-15, https://doi.org/10.1007/978-3-642-03303-2.

[5] Carlo Jacoboni, Theory of Electron Transport in Semiconductors, springer, (2010), p. 76, https://doi.org/10.1007/978-3-642-10586-9.

[6] B.G. Yacobi, Semiconductor Materials, University of Toronto Canada, (2003), p. 59, https://doi.org/10.1007/B105378.

[7] R.A. Smith, Semiconductors 2nd edition, the press syndicate of the University of Cambridge, (1978), p. 103.

[8] Sheng S. Li, Semiconductor Physical Electronics 2nd edition, Springer, (2006), p. 261, https://doi.org/10.1007/0-387-37766-2.

[9] P. Hervb and L. K. J. Vandamme, General relation between refractive index and energy gap in semiconductors, Infared Phys & Technol, Vol 35, N° 4, (1994), p. 609-615, https://doi.org/10.1016/1350-4495(94)90026-4.

[10] V. P. Gupta and N.M. Ravindra, Comments on the Moss Formula, phys. stat. sol. (b), 100, N° 2, (1980), p. 715-719, https://doi.org/10.1002/pssb.2221000240.

[11] N. M. Ravindra, S. Auluck, V. K. Srivastava, On the penn Gap in Semiconductors, Phys. Stat. Sol. (b), 93, N° 2, (1979), p. 155-160, https://doi.org/10.1002/pssb.2220930257.

Chapter III:

[1] Y.C. Ding, A.P. Xiang, M. Xu, W.J. Zhu, Electronic structures and optical properties of γ-Si3N4 doped with La, Physica B, 403, N° 13-16, (2008), p. 2200–2206, https://doi.org/10.1016/j.physb.2007.11.025.

[2] Yan-Xiao Han, Chuan-Lu Yang, Li-Zhi Wang, Mei-Shan Wang, Xiao-Guang Ma, Novel optical properties of γ-Si3N4 with B dopant, Materials Chemistry and Physics, 161, (2015), p. 170-174, https://doi.org/10.1016/j.matchemphys.2015.05.032.

[3] Prashant Singh, Manoj K Harbola, and Duane D. Johnson, Better band gaps for wide-gap semiconductors from a locally corrected exchange-correlation potential that nearly eliminates self-interaction errors, Journal of Physics: Condensed Matter, 29, N°42, (2017), https://doi.org/10.1088/1361-648x/aa837b.

[4] T. Ben Nasr, H.Ben Abdallah, R.Bennaceur, First principles study of the electronic and the optical properties of In_6Se_7 compound, Physica B, 405, (2010), p. 3427–3432, https://doi.org/10.1016/j.physb.2010.05.017.

[5] Sheng S. Li, Semiconductor Physical Electronics, Springer Science+Business Media, LLC, (2006), https://doi.org/10.1007/0-387-37766-2.

[6] Evgeny Y. Tsymbal, PHYS-927: Introduction to Solid State Physics, University of Nebraska–Lincoln.

[7] H. Absike, H. Labrim, B. Hartiti, K. Douhou, H. Ez-Zahraouy, Ab initio calculations on electronic, optical, and thermoelectric properties of (Si, Pb) (co)-doped ZnS for solar cell device applications, Journal of Physics and Chemistry of Solids, 132, (2019), p. 10–17.

[8] M. Dadsetani, B. Kianisadr, and H. Nejatipour, First Principles Investigation of the Optical Properties of BN_xP_{1-x} ($0 \leq x \leq 1$) Boron Ternary Alloys, Journal of ELECTRONIC MATERIALS, 44, N°8, (2015), https://doi.org/10.1007/s11664-015-3691-y.

[9] Zhifeng Huang, Fei Chen, Rui Su, Zhihao Wang, Junyang Li, Qiang Shen, Lianmeng Zhang, Electronic and optical properties of Y-doped Si_3N_4 by density functional theory, Journal of Alloys and Compounds, 637, (2015), p. 376–381.